How the sun protection factor (SPF) of sunscreen films change during solar irradiation

Bernard P. Binks[a], Paul D.I. Fletcher[a]*, Andrew J. Johnson[ad], Ioannis Marinopoulos[a], Jonathan Crowther[b] and Michael A. Thompson[c]

[a] *Department of Chemistry, University of Hull, Hull HU6 7RX, UK*
[b] *GSK Consumer Healthcare (UK) Ltd., 980 Great West Road, Brentford, Middlesex, TW8 9GS, UK*
[c] *GSK Consumer Healthcare 184 Liberty Corner Rd, Warren, NJ, 07059, USA*
[d] *Now at GSK, Harmire Road, Barnard Castle, County Durham, DL12 8DT, UK*

*** Corresponding author**
Prof. Paul D.I. Fletcher
Department of Chemistry,
University of Hull, Hull HU6 7RX, UK
Tel. +44(0)1482 465433
Email P.D.Fletcher@hull.ac.uk

Abstract

We have investigated how the sun protection factor (SPF) of different types of sunscreen film varies with "standard" solar irradiation due to photochemical processes. We have used a combination of chemical actinometry, measurement and modelling to estimate the overall quantum yields for the photoprocesses occurring for avobenzone (AVB) and isopentyl *p*-methoxycinnamate (MC) in either propane-1,2-diol (PG) or squalane (SQ) as solvent. Using the obtained parameters, we have developed models to calculate the evolution of the film spectra and derived SPF values for both non-scattering sunscreen films consisting of solutions of multiple UV filters and for highly scattering Pickering emulsion based sunscreen films. Model calculations for all films are in excellent agreement with film spectra measured as a function of irradiation time using different laboratory light sources. Finally, using the estimated parameters and experimentally validated models, we are able to quantitatively predict how the *in vitro* SPF values for different film types containing any set combination of UV filter concentrations will vary with time due to photochemical processes induced by irradiation with "standard" sunlight. This provides a useful tool for the rational design and optimisation of new sunscreen formulations.

Keywords: sunscreen, sun protection factor, photochemistry, emulsions, avobenzone, *p*-methoxycinnamate.

1. Introduction

Sunscreen films are applied to skin to protect it from the harmful effects of solar UV radiation. The active ingredients are commonly a mixture of UV absorbing molecules and small oxide semiconductor particles which absorb, scatter and reflect light. Formulation types include solutions, particle dispersions and emulsions, both water-in-oil (w/o) and oil-in-water (o/w). In end use by consumers, sunscreens are spread on the skin at application rates of 1-2 mg cm^{-2} which correspond to initial mean film thicknesses of approximately 10-20 μm. The sun protection factor SPF of a sunscreen film is defined by

$$SPF = \frac{med_{with\ sunscreen}}{med_{without\ sunscreen}} \quad (1)$$

where med is the minimum erythema dose of sunlight to induce erythema (sunburn) and the subscripts indicate with or without the sunscreen. SPF is most reliably measured *in vivo* but can be estimated *in vitro* by measuring the optical diffuse transmittance T of the sunscreen film as a function of wavelength λ. The estimated SPF is derived from *in vitro* measurements of T(λ) according to

$$SPF = \frac{\int_{290}^{400} E(\lambda)S(\lambda)d\lambda}{\int_{290}^{400} E(\lambda)S(\lambda)T(\lambda)d\lambda} \quad (2)$$

where E(λ) is the erythema action spectrum and S(λ) is the spectral irradiance of terrestrial sunlight under defined conditions [1-5]. Literature values of E(λ) and S(λ), shown in Figure S1, combined with spectrophotometric measurement of T(λ) for a sunscreen film enables estimation of the film SPF. In equation 2, the wavelength integration limits correspond to the combined UVB and UVA wavelength range of 290-400 nm; SPF values corresponding to the UVB (290-320 nm) or the UVA (320-400 nm) ranges[4] are estimated using equation 2 with substitution of the appropriate wavelength integration limits.

Equation 2 provides the basis for a powerful sunscreen formulation tool to estimate the concentrations of different UV filters required to achieve a target set of UVA, UVB and combined SPF values. For all wavelengths, solutions of UV filters (for which light scattering is negligibly small) mostly follow the Beer-Lambert law:

$$A = \varepsilon c d \quad (3)$$

where A is the optical absorbance which is equal to $-\log_{10}T$, ε is the molar extinction coefficient of the UV filter, c is the concentration and d is the optical path length. As noted above, a typical sunscreen formulation contains several different UV filters. At each wavelength, the absorbance of a sunscreen film containing several, non-interacting UV filters is given by

$$A = (\varepsilon_1 c_1 + \varepsilon_2 c_2 + \varepsilon_3 c_3 + \varepsilon_4 c_4 + \cdots)d \quad (4)$$

where ε_1 and c_1 are the extinction coefficient and concentration of UV filter 1 and the summation can be extended to include any number of different UV filters. To predict SPF values, the extinction coefficient versus wavelength is first measured for each UV filter. The

optical path length (d) of the sunscreen film is typically taken to be 20 μm since this corresponds approximately to the film thickness obtained for an application rate of 2 mg cm^{-2}. Using this set value of the path length and the extinction coefficients as a function of wavelength, input values of the concentrations c_1, c_2, etc. for a possible sunscreen formulation yields A as a function of wavelength. In turn, the calculated absorbance spectrum enables the derivation of $T(\lambda)$ and the predicted SPF values. The concentrations of the UV filters can then be varied until the target SPF values are achieved. It should be noted that, for this approach to be accurate, it is important to check that the UV filter solutions obey the Beer-Lambert law over a wide range of concentrations, i.e. that extinction coefficients are constant. This is because typical UV-vis spectrophotometric measurements use low concentrations with high path length cuvettes (typically 1 cm) whereas sunscreen films have path lengths of around 10-20 μm with correspondingly much higher concentrations of the UV filters.

SPF estimation based on *in vitro* measurements and calculations of this type are more convenient, rapid and less expensive than *in vivo* measurement but suffer from severe limitations. Currently, they are not regarded as providing a reliable estimate of the SPF achieved by a sunscreen formulation in end use by a consumer; only time-consuming and expensive *in vivo* measurements are currently accepted as giving an accurate estimate of SPF. The problems with *in vitro* estimates of SPF include the following. Firstly, the procedure outlined above predicts only an *initial* SPF value corresponding to the initial state of the film. However, during use, the SPF of a sunscreen film can change over the typical sunlight exposure time of a few hours and thus *in vivo* measurements (which correspond to time-integrated average values) will be different to *in vitro* estimates corresponding to the initial values. Time-dependent SPF values can result from (i) evaporation of the volatile film components [6-8] (ii) sunscreen film changes due to water immersion [9] and (iii) photochemical changes in the sunscreen film [10-15] driven by solar irradiation. Secondly, prediction of the initial SPF using equations 2-4 generally works well for sunscreen films which consist of simple, single-phase solutions of molecular UV filters in a solvent. For this type of film, the transmitted light intensity is reduced solely by light *absorption* by the dissolved molecules; light *scattering* effects are not significant. However, many practical sunscreen formulations contain dispersed metal oxide semiconductor particles which, in general, both absorb and scatter light significantly. In addition, instead of consisting of a non-scattering molecular solution, the sunscreen film may be in the form of an emulsion containing μm-sized droplets of one solvent in a second, immiscible solvent. Such emulsion films generally scatter light strongly. Equations 2-4 are valid for non-scattering films but are not generally valid for films which both absorb and scatter light; *in vitro* estimates of the SPF for scattering films requires consideration of full scattering theory which greatly increases the complexity and may not be fully tractable in some cases [16].

We have shown recently how evaporation of sunscreen films can cause large SPF changes over the relevant in-use time scale of a few hours [7,8]. We developed and experimentally validated models which enabled the prediction of how the sunscreen film spectrum (and the derived SPF) changes due to film evaporation-induced processes. Following *in vitro* measurements of some input parameters, the model calculations enable explicit prediction of the time variation of SPF of a formulated sunscreen film due to evaporation. In this way, we have been able to overcome one of the limitations noted above and extend the utility of *in vitro* methods to estimate SPF and its variation with time during use. The main aim of the work described here is to tackle one of the additional limitations; in particular to develop and experimentally validate models which allow explicit prediction of

how sunscreen film SPF varies with time due to photochemical changes induced by the solar irradiation experienced in use. The models will extend the sunscreen formulator's toolbox by, following determination of the required input parameters, enabling the prediction of not only the *initial* SPF but also its solar irradiation-induced time dependence for a chosen set of UV filters and their concentrations. We aim to do this for non-scattering solution films of both single and multiple UV filters and for strongly scattering emulsion films.

Most of the extensive literature relating to photochemical processes which affect sunscreen SPF focuses on identifying the photochemical reaction products, elucidating the reaction mechanisms and quantifying the extent of irreversible photo-degradation of the original UV filters which occurs under different conditions. Although yielding important information, many of the fundamental studies use UV filter solution concentrations, path lengths and irradiation conditions which are very different to those in actual sunscreen usage. Other more applied studies use realistic conditions but yield results relating only to specific, individual systems. The available information provides useful qualitative guidance about the relative photo-stabilities of individual sunscreen UV filters but does not currently enable the quantitative prediction of SPF time dependence due to solar irradiation for a sunscreen film with any set composition. The ability to do this would provide sunscreen formulators with a powerful tool and represents an important step towards the rational design of sunscreen formulations with optimum performance. Because actual sunlight varies with time of day, latitude, solar zenith angle and ozone layer thickness, it is necessary to define a "standard" sunlight which is broadly representative of the sunlight experienced by sunscreen users. The obvious choice is the spectral irradiance of terrestrial sunlight $S(\lambda)$ as used to derive initial SPF according to equation 2 and shown in Figure S1. This choice of "standard" sunlight corresponds to the particular set of defined conditions which are listed in the figure legend.

This paper is organised as follows. Following the Experimental (section 2), the Results and Discussion (section 3) is split into five sub-sections. Section 3.1 shows the use of a chemical actinometric method to determine the absolute spectral irradiances of the different irradiation light sources used here. Section 3.2 details how irradiation of solutions of single individual UV filters is used to determine the quantum yields of the various photochemical processes which occur. The evolution of the film spectra and the derived SPF as a function of irradiation time are modelled and compared with experiment to obtain the relevant quantum yields. Section 3.3 compares measured and calculated spectra during irradiation of solution films containing multiple UV filters. Section 3.4 details how the photochemical processes can be modelled for films consisting of a UV filter dissolved in a scattering emulsion film. Again, the model is validated by comparison of measured and calculated film spectra as a function of irradiation time. It is also illustrated how the photochemical rates vary with the emulsion composition. Using the parameters derived from models developed and validated using laboratory light sources, Section 3.5 shows some illustrative predictions of film SPF as a function of irradiation time with "standard" sunlight. Finally, Section 4 summarises the main conclusions.

2. Experimental

2.1 Materials

Four different UV filters were used in this work. Their chemical structures are shown in Figure 1 and their extinction coefficient spectra are shown in Figure S2. 4-*tert*-butyl-4'-methoxy dibenzoyl methane (Avobenzone, abbreviated here as AVB, Sigma-Aldrich,

pharmaceutical secondary standard grade) was used as received. Isopentyl *p*-methoxycinnamate (Neo Heliopan E1000, abbreviated here as MC), bis-ethylhexyloxyphenol methoxyphenyl triazine (Tinosorb S, abbreviated here as BEMT) and diethylamino hydroxybenzoyl hexyl benzoate (Uvinul A Plus Granular, abbreviated here as DHHB) were kindly donated by the industrial sponsor (GSK) and used as received. Squalane (Sigma-Aldrich, 99% purity, abbreviated as SQ) was columned over neutral aluminium oxide (Merck) to remove any polar impurities. Propane-1,2-diol (Sigma-Aldrich, > 99%, abbreviated as PG) was used as received. Reagents for the actinometry measurements, 9,10–Dimethylanthracene (DMA, Sigma–Aldrich, > 99%) and 1,1,2–Trichloro–1,2,2–trifluoro ethane (Freon 113, Sigma–Aldrich, >99.7%) were used as received. The fumed silica particles used for stabilisation of the emulsions had a specific surface area of 200 $m^2\ g^{-1}$ and primary particle diameters of 10–30 nm. They were surface modified by grafting with dichlorodimethylsilane (DCDMS) to obtain particles of different hydrophobicity, expressed as the % of unmodified surface silanol groups present. Samples with 23% and 35% surface SiOH present were provided by Wacker-Chemie (Germany) and used as received.

2.1 Methods

UV/vis spectra were measured using a double beam PerkinElmer Lambda 25 spectrophotometer for samples in quartz cuvettes (Hellma Analytics) of path lengths of 0.01, 0.1 and 1 cm. This instrument measures the *specular* optical transmittance (with subsequent conversion to absorbance) with a detector acceptance angle estimated to be $<5^o$ either side of normal incidence. Using this double-beam instrument, spectra of UV filter solutions or dispersions were measured versus air as reference. Reference spectra of the solvent-filled cuvette versus air were separately measured. Spectra of the UV filters alone were obtained by subtraction of the reference spectrum from the sample spectrum.

UV irradiation experiments were made using either a UV lamp or a solar simulator. The UV lamp measurements used a B7960 lamp from Agar Scientific having two cylindrical 6 W Hg tubes emitting at wavelengths around 360 nm. Irradiation samples in quartz cuvettes were mounted horizontally at fixed positions underneath and parallel to the lamp tubes. The samples were irradiated within a rectangular opaque box which was thermostatted at 32^oC. Three different sample-UV lamp distances (3.6, 7.2 and 14.4 cm) were used to vary the light intensity incident on the samples. Solar simulator measurements were made using an Oriel Solar Simulator (Model 81291) operating at 200 W/10 A and fitted with the Atmospheric Attenuation Filter (No 81017). The illuminated area was 10 x 10 cm with a parallel, collimated beam. Although it was checked that the light output intensity was independent of the sample location distance from the light exit lens, all measurements were made using a constant sample-lens distance of 55 cm. Emission spectra of the UV lamp at all sample-lamp distances and the solar simulator were measured using a Thorlabs OSA Compact Spectrophotometer (CCS200/M). The light was directed straight into the spectrometer; no fibre optic was used. The software used with this spectrometer applies a factory-set response function such that the output corresponds to the relative light intensity as a function of wavelength.

Silica particle-stabilised emulsions containing squalane (SQ) and propane-1,2-diol (PG) were prepared as follows. The masses of the two liquids and the silica particle powder required to produce approximately 10 cm^3 of emulsion were added to glass vessels of 28 mm diameter by 72 mm height. Each mixture was emulsified using an IKA Ultra–Turrax T25 homogeniser with a rotor-stator head of 18 mm diameter operating at 13,000 rpm for 2

minutes at room temperature (21°C). For each emulsion sample, the emulsion type (SQ-in-PG or PG-in-SQ) was determined shortly after preparation by observing whether a drop of the prepared emulsion dispersed or not when added to either pure PG or pure SQ. Optical micrographs of the emulsion were obtained using an Olympus BX51 microscope equipped with an Olympus DP70 camera and ImageJ software. Emulsion drop size distributions were obtained from the micrograph images by analysis of not less than 50 drops on each image.

Except where noted otherwise, all measurements were made at 32°C since this is the surface temperature of human skin.

3. Results and Discussion

A key aim of this study is to be able to predict the variation of sunscreen film absorbance spectra and derived SPF as a function of irradiation with "standard" sunlight. To re-iterate the steps we use to achieve this: we first use actinometry to convert the measured relative light intensities as a function of wavelength for the light sources used here into the absolute spectral irradiances. Secondly, we irradiate sunscreen films with these light sources of known spectral irradiance to obtain the various quantum yields corresponding to the different photochemical processes occurring. Finally, we use the quantum yields and the known spectral irradiance of "standard" sunlight to calculate spectra and SPF for sunscreen films during solar irradiation.

3.1 Actinometric estimation of the spectral irradiances of the light sources used here

In this first step, we irradiate an actinometric system with known quantum yields to obtain the spectral irradiances of the light sources. The relevant photochemical theory is as follows [17,18]. We consider a simple photochemical reaction reactant + photon → product which is implemented by irradiation of a cell containing the reactant with an optical path length d. For photochemical reactions, it is convenient to discuss the rate of the reaction per unit time *per unit illuminated cell area* (units: mol m^{-2} s^{-1}) as opposed to the rate of change of solution concentration per unit time as used in non-photochemical reaction kinetics. For polychromatic irradiation the rate is:

$$rate = \int \phi(\lambda)\, I_a(\lambda) d\lambda \qquad 5$$

where $\phi(\lambda)$ is the wavelength-dependent quantum yield for the reaction and $I_a(\lambda)$ is the number of moles of irradiating photons of wavelength λ absorbed by reactant A per unit time per unit illuminated area per unit wavelength. The overall reaction rate is obtained by integration over the wavelength range of the light source. $I_a(\lambda)$ is related to the number of moles of photons incident on the sample per unit area per unit time per unit wavelength $I_o(\lambda)$ according to

$$I_a(\lambda) = 0.96 I_o(\lambda)\left(1 - 10^{-A_{reac}(\lambda)}\right) \qquad 6$$

where $A_{reac}(\lambda)$ is the optical absorbance due to the reactant species and 0.96 is a correction factor to account for light transmittance losses due to reflection at the front face of the irradiation cell. Equation 6 is valid for systems in which only the reactant species absorbs in the wavelength range of interest. For systems containing additional absorbing "spectator"

species with absorbance $A_{spec}(\lambda)$, equation 6 is modified to take account of the light transmittance losses due to absorption by the "spectator" species:

$$I_a(\lambda) = 0.96 I_o(\lambda)\left(1 - 10^{-A_{reac}(\lambda)}\right)\frac{\left(1 - 10^{-A_{spec}(\lambda)}\right)}{A_{spec}(\lambda)\ln(10)} \qquad 7$$

The incident photon flux $I_o(\lambda)$ is related to the spectral irradiance of the light source $S(\lambda)$ by

$$I_o(\lambda) = \frac{S(\lambda)\lambda}{hcN} \qquad 8$$

where h is Planck's constant, c is the speed of light and N is Avogadro's number. Using equations 5-8, the overall photochemical reaction rate can be predicted so long as $S(\lambda)$ for the light source and the quantum yields and absorbance spectra of all reactant and spectator species are known.

To obtain $S(\lambda)$ for the light sources used here, we measure the *relative* light emission intensity as a function of the wavelength $I(\lambda)$ in arbitrary units which is expected to be proportional to $S(\lambda)$. The constant of proportionality is obtained by comparison of measured and calculated photochemical reaction rates for an actinometric reaction for which the quantum yields $\phi(\lambda)$ are known. Using the excellent compendium of different actinometric reactions by Kuhn et al. [19], the actinometric reaction selected was the self-sensitised photo-oxygenation reaction of 9,10-dimethyl-anthracene (DMA) in air-saturated Freon solvent [20]. The quantum yield for this reaction is independent of wavelength over the range 334-395 nm and equal to 0.58±0.02. DMA solutions were irradiated with each light source used here and the evolution of the UV-vis spectrum recorded. The initial overall reaction rate is derived from the measured initial rate of absorbance change according to

$$rate = -\frac{\frac{dA}{dt}}{\varepsilon_{reactant} - \varepsilon_{product}} \qquad 9$$

where ε is the molar extinction coefficient of the subscripted species. For the DMA reaction, $\varepsilon_{reactant}$ was obtained from the measured DMA absorbance spectrum prior to irradiation. The reaction products do not absorb light over the monitoring wavelength range, i.e. $\varepsilon_{product}$ is zero and so the rate = $-(dA/dt)/\varepsilon_{reactant}$. Although the rate of absorbance decrease $-(dA/dt)$ is wavelength dependent, the values of measured initial reaction rate derived using equation 9 were found to be virtually identical for all monitoring wavelengths over the range 320-400 nm. The final value of the measured initial reaction rate was taken as the average over this monitoring wavelength range.

The overall initial rates were calculated using equations 5-8 with integration over the irradiation wavelength range of 250-450 nm using a guessed value of the constant of proportionality between $I(\lambda)$ and $S(\lambda)$. This constant was adjusted until the measured and calculated initial rates agreed. Figure 2 shows one example of the DMA spectra obtained during irradiation which was used to obtain the constant of proportionality. Having obtained the constant in this way, it was used with the measured $I(\lambda)$ to derive $S(\lambda)$ versus wavelength for the different light sources used. The lower plot of Figure 2 compares the spectral

irradiances of the different light sources used here with S(λ) for "standard" terrestrial sunlight.

3.2 Photochemical kinetics of solutions of a single UV filter

Having obtained the absolute spectral irradiances of the light sources, they were used to irradiate solutions of each of the four UV filter species with the structures shown in Figure 1. Extensive irradiation of BEMT and DHHB solutions produced no changes in the spectra of their solutions and it was concluded that both these molecules are photostable. The photochemical properties of AVB and MC in either PG or SQ as solvent are discussed in detail below.

The photochemistry of AVB and related, chemically-similar species has been extensively investigated [21-33]. Prior to irradiation, AVB solutions in different solvents generally contain a mixture of >90% enol and <10% keto forms (see Figure 1). Neglecting discussion of short-lived, transient rotamer intermediates, the basic photochemical behaviour of AVB can be briefly summarised as follows. UV irradiation causes the enol form (with peak absorbance around 360 nm) to convert to the keto form with peak absorbance around 260 nm. In some solvents, the keto can convert back to the enol in a dark reaction but this is not observed here for AVB in either PG or SQ as solvent over storage in the dark for more than 24 hours. Continuing irradiation of the keto gives a Norrish type I cleavage of the keto form to yield radicals which form a variety of final products which mostly absorb only at wavelengths below about 280 nm [27].

Figure 3 shows the spectra of an AVB solution in squalane as a function of irradiation time. It can be seen that the peak around 360 nm (due to the enol species) decreases and the peak around 262 nm (due to the keto species) increases with irradiation time. It can also be seen that the spectra cross over at several wavelengths. However, close examination reveals that the cross over points are not true isosbestic points which would be observed if the only process occurring was the conversion from enol to keto forms and the solutions contained only mixtures of these two species. The lack of isosbestic points indicates that more than two species contribute to the overall absorbance. Overall, the spectra are consistent with previous observations that two main photo processes occur sequentially. The enol form is converted to the keto form which, in turn, is converted to a mixture of final photo products. For the analysis described below, we treat the mixture of final photo products as a single species which we denote here as "prod". In order to obtain the quantum yields for these two processes, it is first necessary to estimate the individual extinction coefficient spectra for the enol, keto and prod species. For each wavelength, the total absorbance A is the sum of the contributions from the enol, keto and prod species according to:

$$A = (\varepsilon_{enol}[enol] + \varepsilon_{keto}[keto] + \varepsilon_{prod}[prod])d \qquad 10$$

where ε is the (wavelength-dependent) extinction coefficient of the sub-scripted species and d is the path length. The sum of the concentrations of the enol, keto and prod species is equal to the initial overall concentration of AVB. Using the Solver function in Excel, all the absorbance spectra as a function of irradiation time were calculated using equation 10 using guessed values of the concentrations of enol, keto and prod species and all the extinction coefficients for all three species over the wavelength range 235-400 nm. The calculated spectra were compared with the measured spectra and the sum of absolute differences computed. The residual sum between the global set of measured values of A and those

calculated using equation 10 was then minimised by adjustment of all the unknown parameters. This procedure involves fitting a total of over 500 unknown parameters; we note here that Solver allows only fitting of a maximum of 200 unknown parameters and so the fitting was performed in several stages. Despite this large number of fitting parameters, it was found that the fit procedure successfully converged to a solution for which the average deviation between measured and calculated values of the overall absorbance was approximately equal to the experimental uncertainty in the measured absorbance (approx. 0.003 absorbance units). It was checked that consistent fits were obtained when starting the fitting procedure from widely different initial parameter values. In addition, independent fitting of data sets corresponding to either 8 mM AVB with 0.01 cm path length (Figure 3) or 0.045 mM AVB with 1 cm path length (not shown) yielded self-consistent values of the extinction coefficients.

For the 8 mM AVB with 0.01 cm path length data set, Figure 3 shows the fitted values of the species' concentrations as a function of irradiation time. As noted above, the solution prior to irradiation contains mostly the enol form with only a small fraction of the keto form. Using the procedure described here, we find that AVB solutions in SQ initially contain approximately 5% of the keto form and PG solutions approximately 3% keto. These values are similar to those obtained using NMR for AVB in different deuterated solvents for which values were in the range 1-9% [32]. Consistent with the proposed sequence of photo-processes, the enol concentration decreases monotonically, the keto form concentration initially increases and then decreases. The product concentration remains zero initially (when the keto concentration is low) and then increases steadily. The final derived extinction coefficient spectra are shown in the lower plot of Figure 3. The same fitting procedure was applied to AVB solutions in PG. As seen in Figure S3, AVB behaves qualitatively similarly in PG although it can be seen that the rates of the AVB photochemical processes are slower in PG as compared with SQ. For both solvents, the spectra of the enol and keto forms are accurate but the spectra of the product species have relatively large uncertainties since, particularly in PG as solvent, the maximum conversion to product is low and hence its effect on the overall measured absorbance is small. The small absorption of the product species observed here for wavelengths greater than 250 nm is consistent with the observations described in ref. [27]. The extinction coefficient spectra of the enol and keto forms estimated here for AVB in SQ and PG are similar to the spectra reported for AVB and methylated derivative in acetonitrile [28].

Having obtained the extinction coefficient spectra of the species present during irradiation, the evolution of the spectra as a function of irradiation time can be calculated using input values of the quantum yields for the enol to keto and the keto to product photo-processes. Best-fit values of the quantum yields are obtained by adjustment of the values until agreement is observed between the calculated and measured spectra as a function of irradiation time. The calculation procedure used is detailed in the supplementary information. Figure 4 shows an illustrative example of the comparison between measured and calculated spectra obtained using this fitting procedure to obtain the two quantum yields. The measured and calculated spectra are in good agreement. Overall, the good quality of the fitting is most clearly seen by the excellent agreement between the SPF values derived from the measured and calculated spectra. The same fitting procedure was applied to six different data sets obtained using irradiation with the UV lamp at 3.6, 7.2 and 14.4 cm and the solar simulator, with AVB concentrations ranging from 0.045 to 12 mM and path lengths from 0.0018 to 1 cm. For the enol to keto reaction, the quantum yields obtained were consistent within an estimated uncertainty of 50% (standard deviation/mean). Since the keto to prod

reaction produces smaller changes in the spectra, the uncertainty in this quantum yield is higher and approaches 100% (standard deviation/mean). The final values are listed in Table 1. Although the quantum yields obtained from the different runs were somewhat variable (giving the relatively high uncertainties in the final averaged values), it was checked that the values from individual runs showed no systematic trends with either AVB concentration or with the irradiation light source used. We conclude here that the relatively high observed uncertainties probably result from random variability in the emission outputs of the light sources used.

Similar data sets including both light sources, widely differing concentrations and path lengths were measured and fitted for AVB in PG as solvent. One example is shown in SI Figure 4 where it can be seen that the overall rate of change of the AVB spectrum is approximately three times slower in PG compared to SQ. Final values of all quantum yields, averaged over all the individual runs, are listed in Table 1. When comparing the spectral changes for AVB in SQ and PG when irradiated with the same light source, the main spectral changes (due to the enol to keto process) occur approximately five times slower in PG. As shown in Table 1, this effect corresponds to the enol to keto quantum yield being approximately five-fold less in PG than in SQ. However, the quantum yields for the keto to prod reaction are similar in both PG and SQ.

AVB is used in sunscreen formulations mainly to block UV-A radiation in the wavelength range 320-400 nm. However, this function is performed only by the enol form of AVB. As seen in Figures 4 and S4, the SPF corresponding to UV-A is initially high relative to the UV-B SPF and combined SPF values. During irradiation causing mainly the enol to keto conversion, the UV-A SPF decreases fairly rapidly in SQ and more slowly in PG. The UV-B and combined SPF values both remain virtually constant during irradiation.

We have also applied the procedure described above to solutions of MC in both SQ and PG. Again, the photochemistry of MC and structurally-similar derivatives have been extensively discussed in the literature [23,29,30,34-39]. As received, MC consists entirely of the trans isomer. Irradiation of the trans isomer causes its conversion to the cis form (see Figure 1). Simultaneously, irradiation of the cis form drives its conversion back to the trans form. The result of these two processes is that the trans/cis ratio changes during continuous irradiation from its initial value of 100% trans to reach a steady-state value in which the photochemical rates of the cis to trans and trans to cis balance. Subsequently, the cis/trans ratio does not change with further irradiation. For both SQ and PG as solvent, it was observed here that the spectra of the irradiated (steady-state) MC solutions did not change further when left in the dark for 24 hours, i.e. the irradiated mixture of cis and trans forms did not revert back to the original 100% trans form.

Figure 5 shows the spectral changes for MC in PG upon irradiation together with the fitted values of the concentrations and extinction coefficient spectra of the cis and trans species. Unlike those for AVB, the isosbestic points in the measured MC spectra appear accurately maintained; this is consistent with the idea that only two absorbing species are present. During irradiation, the trans/cis ratio initially decreases until the final steady-state value is reached. The derived extinction coefficient spectra of the cis and trans species are similar to those reported for octylmethoxycinnamate in different solvents [36,37,39]. Qualitatively similar behaviour (not shown) was found for MC in SQ.

Similarly to the procedure used for AVB, the extinction coefficient spectra were used to calculate the spectra and SPF values as a function of irradiation time using guessed values of the trans to cis and cis to trans quantum yields. Minimisation of the residual sum computed from comparison between measured and calculated spectra yielded the "best-fit" values of both quantum yields. Figure 6 gives an illustrative example showing the excellent fit obtained between the measured and calculated spectra and the corresponding derived SPF values for an individual run. Similar fits were obtained for runs using the UV lamp at the different distances and the solar simulator and MC solutions with concentrations ranging from 0.08 to 6 mM and path lengths in the range 0.01 to 1 cm. Quantum yields from all runs in PG and a similar set of runs in SQ (not shown here) yield the final averaged values shown in Table 1. Compared with the values for AVB, the quantum yields for MC are two to three orders of magnitude larger with the result that, for equivalent levels of irradiation, the MC photochemical process rates are much faster. A second difference relates to the solvent dependence. For AVB, the rates are faster in SQ compared to PG whereas the opposite is true for MC. Finally, we note that the two quantum yields for MC in PG add up to more than one. This implies that the cis to trans and trans to cis photo isomerizations do not share a common transition state. The magnitudes of the quantum yields estimated here are broadly similar to the values reported for octyl methoxycinnamate in various solvents [34,39].

MC absorbs mainly UV B light (290-320 nm). Hence, as seen in the lower plot of Figure 6, irradiation causes a fairly rapid decrease in the UV B SPF to a plateau value but causes virtually no change in the (low) value of the UV A SPF.

3.3 Photochemical kinetics of solutions of multiple UV filters

Practical sunscreen formulations generally contain more than one UV filter present in formulated mixtures designed to provide optimum protection against both UVA and UVB radiation. Using measured extinction coefficient spectra of all the UV filters present, it is simple to predict the spectra, and hence all derived *initial* SPF values, for a sunscreen film containing set concentrations of the different UV filters. This is a useful formulation tool but it fails to predict how the initial SPF values change during solar irradiation. To address this, we have measured how the irradiation behaviour of AVB solutions change when mixed with different concentrations of BEMT which acts as a photostable "spectator" species.

Figure 7 compares the measured and calculated spectra as a function of irradiation time for one of the AVB/BEMT mixtures. Excellent agreement is observed. As predicted by equation 7, the addition of BEMT to the AVB solution film reduces the intensity of the irradiating light and thus slows down both AVB photo-processes. This slowing effect is seen in the upper plot of Figure 8 which shows the variation of measured and calculated SPF for 2.5 mM AVB with and without the addition of 2.23 mM BEMT. Excellent agreement is observed between SPF values derived from the measured and from the calculated spectra for the films with and without the added BEMT. The addition of BEMT increases the initial SPF and also alters the relative magnitudes of the UVA (320-400 nm), UVB (290-320 nm) and total SPF (290-400 nm) values. Importantly, the fitting/simulation procedure also correctly predicts the time variation of the different SPF values from which it can be seen that the addition of BEMT slows down the changes in SPF. This slowing effect is more evident in the lower plot of Figure 8 which shows how the AVB enol, keto and product species' concentrations change during irradiation. The rates of loss of enol, gain of keto and gain of the final product are reduced by approximately two-fold by the addition of the BEMT at the concentration used. Results for different mixtures of AVB and BEMT (not shown) showed

similar agreement between measured and calculated spectra and consistent values of the two quantum yields for AVB.

3.4 Photochemical kinetics of UV filters in emulsions

So far, we have considered sunscreen films consisting of solutions which absorb but do not scatter light. However, many commercial sunscreens contain one or more UV filters dissolved in a light scattering emulsion which can consist of either water (or another polar solvent) droplets in an apolar oil or oil droplets in water. It is therefore important to elucidate how light scattering from an emulsion affects SPF and its time evolution during irradiation. To tackle this problem, we have investigated how UV irradiation changes the spectra of either AVB or MC dissolved within emulsions of PG and SQ stabilised by partially hydrophobised silica nanoparticles. Figure 9 shows optical micrographs of PG-in-SQ and SQ-in-PG emulsions, both with 50 vol% PG and containing no UV filter. It was checked that the emulsions were stable over the duration of the irradiation experiments and that the stability and mean droplet sizes were not affected by either inclusion of AVB or MC and by variation of the volume fraction of PG.

As measured using light microscopy, the emulsion droplets are polydisperse with number average diameters of 20 and 18 μm for the SQ-in-PG and PG-in-SQ types respectively. They scatter light and have a greyish/whitish visual appearance when viewed in a sample tube. Whether or not the light scattering from a thin sunscreen film contributes to a loss of transmitted light intensity (and hence an increase in the SPF) depends on the details of how the light is scattered. Light scattered at forward scattering angles of $<90^o$ is transmitted through the sunscreen film and therefore does *not* contribute to an increase in SPF. Only back scattered light (i.e. light scattered at scattering angles $>90^o$) is not transmitted through the film and therefore contributes to an increase in SPF. Experimentally, one can use a spectrophotometer equipped with an integrating sphere to determine the *diffuse* transmittance, i.e. the fractional light intensity transmitted over the scattering angular range $\pm 90^o$ when using plane parallel incident light normal to the sample. The diffuse absorbance is derived as the negative logarithm of the diffuse transmittance. As noted in the Introduction, the derivation of SPF from transmittance measurements as a function of wavelength requires the use of the diffuse transmittance (more exactly, the diffuse transmittance not including the back scattered light). Conventional UV-vis spectrophotometers (as used here) record the absorbance derived from the measured *specular* transmittance, i.e. the fractional light intensity transmitted over a narrow scattering angular range close to zero. For samples which absorb but do not scatter light significantly, the diffuse absorbance is equal to the specular absorbance. Hence, for sunscreen films consisting of non-scattering solutions, the SPF is correctly derived from measurements of the specular absorbance spectra using a conventional specular spectrophotometer. For emulsion films which scatter light, specular absorbance measurements will not yield the correct derived SPF values.

The emulsions used here contain droplets which are large relative to the wavelength range of the incident light. These large scattering objects scatter light strongly in the forward direction, i.e. over a narrow range of scattering angles close to zero. As seen in Figure S5, Mie scattering theory/software [40] was used to calculate the angular distribution of the light scattered by a range of different droplet sizes. For droplet sizes around 20 μm as in the emulsions used here, the light is scattered within a small scattering angular range of $\pm 2^o$. Part of this scattered light falls outside the detector acceptance angular range of the specular spectrophotometer used here and thus is recorded as a contribution to the overall absorbance.

As seen in Figure 10, the contribution to the measured specular absorbance resulting from the light scattered from a 0.01 cm thick SQ-in-PG emulsion film is approximately 0.7-1 across the wavelength range 200-400 nm. When the absorbance spectra of these same emulsion films are measured using a diffuse spectrophotometer with an integrating sphere with detector acceptance angular range of $\pm 60^{o}$, virtually all of the scattered light is detected and hence the reported diffuse absorbance due to scattering is zero[8]. For sunscreen film samples which both absorb and scatter light, there is an additional important consideration. If the light scattering occurs at large forward angles, the scattered photons experience a light path through the sample which is significantly larger than the cell path length. In this case, the component of light which is scattered will experience additional absorption due to its longer light path. For small forward scattering angles, the light absorption experienced by the scattered light will be virtually the same as the non-scattered light. The light path of the scattered light can also be increased by multiple scattering which occurs when the overall scattering is large [41].

As a result of the considerations discussed above, the absorbance spectra of these emulsions containing a UV filter measured using a specular spectrophotometer are expected to consist of a contribution due to scattering at angles greater than the detector angular acceptance range plus a contribution due to light absorption. Because the scattering angles are small and the scattered light paths are virtually equal to the cell path length, this latter absorption contribution is expected to be virtually identical to that observed for a non-scattering film of the same composition. As seen in Figure 10, this expectation is confirmed by the fact that the measured spectrum prior to irradiation agrees with that calculated using the extinction coefficient spectrum of the UV filter measured in solution and the separately measured absorbance spectrum of the emulsion alone (due solely to scattering). Additional confirmation of this conclusion is shown in ref. [8] in which the measured diffuse and specular spectra of these emulsion films are compared.

Having established that the emulsion scattering in these films does not affect the absorbance due to light absorption, we can now model how the spectrum changes during light irradiation. We consider AVB dissolved in an emulsion containing a volume fraction of PG equal to ϕ_{PG} and a volume fraction of SQ equal to $(1 - \phi_{PG})$. As discussed earlier, light irradiation of AVB causes the two photochemical reactions enol to keto and keto to prod and both reactions have quantum yields which are different in PG and SQ. During irradiation, three species are present (enol, keto and prod), each of which will partition between the PG and SQ liquid phases within the emulsion. Hence, we must consider a total of six species which are $enol_{PG}$, $enol_{SQ}$, $keto_{PG}$, $keto_{SQ}$, $prod_{PG}$ and $prod_{SQ}$ which all have different extinction coefficients (ε_{enolPG}, ε_{enolSQ}, etc.) as a function of wavelength. It is assumed here that the species' partitioning is fast relative to the photochemical reactions and so the ratio of PG and SQ concentrations of each species is maintained equal to the equilibrium value of the relevant partition coefficient according to:

$$P_{enol} = \frac{[enol_{SQ}]}{[enol_{PG}]} \qquad 11$$

where P_{enol} is the equilibrium partition coefficient for the enol species and the square brackets indicate the concentration of the species with respect to the volume of indicated liquid phase. Similar equations are valid for the keto and prod species. For each of the three species, the total concentration of each individual species with respect to the total volume of emulsion $C_{species,tot}$ is related to the concentration of the species in PG ($C_{species,PG}$) according to

$$C_{species,tot} = (\phi_{PG} + (1 - \phi_{PG})P_{species})C_{species,PG} \quad 12$$

The concentrations with respect to the total emulsion volume (denoted using C with the appropriate subscripts) are related to the concentrations with respect to the volume of the relevant liquid phase (denoted with the square brackets) by the equations

$$C_{species,PG} = \phi_{PG}[species_{PG}] \; and \; C_{species,SQ} = (1 - \phi_{PG})[species_{SQ}] \quad 13$$

The total of all species concentrations is equal to the initial, overall concentration of AVB. The evolution of the overall absorbance spectrum and derived SPF during irradiation was calculated using the procedure shown in the supplementary information. As seen in Figure 10, the agreement between the measured and calculated spectra for a SQ-in-PG emulsion film with ϕ_{PG} = 0.5, 5 mM AVB and path length of 0.01 cm is excellent. According to the theory presented above, the photochemical behaviour is predicted to depend on ϕ_{PG} but not on whether the emulsion type is SQ-in-PG or PG-in-SQ. Changing the emulsion type is predicted to have no effect on the evolution of the specular absorbance spectrum due to light absorption but may have an effect on the specular absorbance "baseline" due to the emulsion scattering. To test this prediction, we have measured and modelled the spectra for a PG-in-SQ emulsion film with ϕ_{PG} = 0.5, 5 mM AVB and path length of 0.01 cm. As seen in Figure S6, the spectra as a function of irradiation time are very similar to those of Figure 10; the only differences are due to changes in the specular absorbance due to the emulsion alone. Again, the agreement between measured and calculated spectra is excellent. Best-fit values of P_{enol} and P_{keto} derived from both types of emulsion are listed in Table 3 and show reasonably good agreement. In addition, the best-fit values of P_{enol} are similar to the value derived from the ratio of AVB solubilities in the two solvents (see Table 2).

Similar measurements and modelling were done for emulsion films containing MC for which irradiation drives photo-reversible trans/cis isomerisation. In the case of MC in an emulsion film, only four species ($trans_{PG}$, cis_{PG}, $trans_{SQ}$ and cis_{SQ}) have to be considered. For the simulations, the four relevant quantum yields listed in Table 1 were used. The partition coefficients P_{trans} and P_{cis} were the only unknown parameters floated in the modelling. An illustrative example of the comparison between measured and calculated spectra during irradiation is shown in Figure S7 where it can be seen that the agreement is again very good. As seen in Table 3, the best-fit values of P_{trans} and P_{cis} obtained from the two emulsion types were in reasonable agreement. The best-fit values of P_{trans} are somewhat lower than the values corresponding to the ratio of solubilities but this may be a consequence of the high solubilities of MC in these solvents which is likely to cause deviation from ideal solution behaviour.

We have demonstrated that the photochemical parameters derived from measurements made using solution films successfully predict the photochemical behaviour of both AVB and MC in emulsion films. The analysis reveals that the photochemical rates depend on the emulsion composition (i.e. ϕ_{PG}) but do *not* depend on the emulsion type or other parameters such as the mean emulsion drop size (so long as the light scattering conditions discussed above apply). For the purposes of showing more clearly how the emulsion sunscreen formulation variable ϕ_{PG} affects the photochemical rates, we have measured how the relevant rate parameters for both AVB and MC vary in emulsions with different volume fractions of PG. PG-in-SQ emulsions with ϕ_{PG} in the range 0.2-0.6 were stabilised with 1 wt% of 23

%SiOH silica particles and SQ-in-PG emulsions with ϕ_{PG} in the range 0.4-0.8 were stabilised with 1 wt% of 35 %SiOH silica particles. All emulsions were stable and had mean drop sizes in the range 18-20 μm.

For irradiation of strongly absorbing AVB-containing films with a constant light source, the peak absorbance due to the enol form initially decreases linearly due to the enol to keto photo reaction. Hence the initial reaction rate is proportional to the enol to keto quantum yield which is 0.4×10^{-4} in pure PG and 2×10^{-4} in pure SQ. The initial reaction rate r in the emulsion films is taken to be equal to the volume fraction weighted initial rates in each of the pure solvents according to

$$r = \phi_{PG} r_{PG} + (1 - \phi_{PG}) r_{SQ} \qquad 14$$

where r_{PG} is the initial rate in pure PG and r_{SQ} is that for pure SQ. Hence, the initial rate for AVB is predicted to decrease approximately 5-fold as ϕ_{PG} is increased from 0 to 1. For irradiation of MC-containing emulsion films, the peak absorbance (due to the trans form) decreases exponentially to a plateau value corresponding to the photo-stationary state mixture of trans and cis forms [39]. Fitting the peak absorbance decrease as a function of irradiation time to an exponential function yields a first-order rate constant k. This rate constant is proportional to the sum of the trans-cis and cis-trans quantum yields and is 0.16 + 1.0 = 1.16 for pure PG and 0.028 + 0.10 = 0.128 for pure SQ. In emulsion films, k is taken to be equal to the volume fraction weighted values in each of the pure solvents according to

$$k = \phi_{PG} k_{PG} + (1 - \phi_{PG}) k_{SQ} \qquad 15$$

Hence, k for MC is predicted to increase approximately 9-fold as ϕ_{PG} is increased from 0 to 1. Figure 11 compares the variation of the measured and calculated AVB initial rates and MC k values as a function of ϕ_{PG}. Both plots include values measured in both PG-in-SQ and SQ-in-PG emulsion films and non-emulsion (solution) films and include measurements with different path lengths and concentrations of the UV filter. Although the spread in values are fairly large (reflecting the relatively large experimental uncertainties noted earlier), the agreement between the measured data and the predictions of equations 14 and 15 is reasonably good. The plots reveal how control of the emulsion composition can be used to vary the extent of photochemical change in an emulsion sunscreen formulation.

3.5 Prediction of the SPF changes during solar irradiation

Having used actinometry to obtain the absolute spectral irradiances of the light sources used here, we have been able to estimate the quantum yields for the different photochemical process occurring in AVB and MC in both PG and SQ as solvents. Although the estimated quantum yields have been assumed to be wavelength independent over the wavelength range 250 to 400 nm and have fairly high uncertainties, consistent values have been obtained for the different light sources used, solutions with widely differing path lengths and UV filter concentrations, solutions containing mixtures of different UV filters and in emulsion films. We now use the values of the quantum yields to predict how the spectrum of a sunscreen film and the different SPF values will vary with exposure to "standard" sunlight. In order to be consistent with *initial* SPF values derived using the S(λ) shown in Figure S1, we use this same S(λ) as "standard" sunlight to calculate the variation of SPF with duration of sun exposure.

The models developed here together with the required input data of quantum yields and extinction coefficient spectra enable calculation of the spectra, SPF and species' concentrations for single and multiple UV filter solution and emulsion films with any set concentrations and path length (equal to sunscreen film thickness) as a function of irradiation time. We illustrate the calculations with results for solution films of either AVB or MC which are both photo-unstable. Figure 12 shows the calculation results for 20 μm films of 30 mM AVB in either SQ or PG during solar irradiation over a four hour period. We note here that the solubility of AVB in PG is only 14 mM and so a 30 mM AVB solution in this solvent is not achievable; however, we retain this calculation in order to better compare AVB behaviour in the two solvents. AVB, with peak absorbance around 360 nm, is mainly used in sunscreen formulations to provide protection against UVA radiation. It can be seen that the initial values of SPF 320-400 nm are high whereas SPF 290-400 and SPF 290-320 are relatively low. However, solar irradiation converts the enol to the keto form which has the effect of decreasing SPF 320-400 while having relatively little effect on the other SPF values. Owing to the different quantum yields in PG and SQ, this loss of UVA SPF is relatively fast in SQ (the UVA SPF decreases from 11 to 5 in 4 hours) but is slower in PG. The calculations also provide an estimate of the enol, keto and product species' concentrations during solar irradiation. This latter aspect is potentially useful since it gives an estimate of the actual amounts of potentially toxic final photoproducts produced in the end use of a sunscreen.

Figure 13 shows similar calculations for 20 μm films of 30 mM MC in either SQ or PG during solar irradiation over a 20 minute period. MC, with peak absorbance around 320 nm, mainly provides protection against UVB radiation and the films give initial high values of SPF 290-320 and low values of SPF 320-400. Irradiation of MC causes photo-reversible cis-trans isomerisation to reach a photostationary state with a constant cis/trans ratio. Relative to the photoprocesses for AVB, MC reacts much faster (over minutes compared with hours for AVB) as a result of the higher quantum yields. For MC in SQ as solvent, the quantum yields are such that the photostationary state is achieved very fast (within 2 minutes or so) but the extent of conversion from trans to cis forms is small. As a result, the UVB SPF shows a fast but small initial change. In PG as solvent, the photostationary state is achieved approximately ten times slower (after 20 minutes or so) but the extent of conversion from trans to cis is much greater. Thus, the UVB SPF shows a large decrease from 13 to 5 over the first 20 minutes irradiation. The UVA SPF is small and remains virtually constant during irradiation. These predicted differences of the behaviour of MC in the two solvents are a consequence of the fairly small differences in the cis and trans extinction coefficient spectra between the two solvents leading to larger differences in their overlap with the solar emission spectrum.

Similar model calculations are possible for solution and emulsion films containing single or multiple UV filters at any set concentrations and path length (equal to the film thickness) so long as the relevant input parameters (extinction coefficient spectra and quantum yields) are known. This enables *in vitro* estimation of not only *initial* values of SPF but also their time dependence due to solar irradiation.

4. Conclusions

We have investigated solution and sunscreen films containing different combinations of four UV filters and two solvents. We have shown that DHHB and BEMT are photo-stable whereas irradiation of AVB and MC causes their spectra to change as a result of

photochemical processes which have been established previously. Using irradiation light sources calibrated using actinometry, we have measured the spectra of solution films of either AVB or MC as a function of irradiation time. Computer fitting of these spectra yielded both the extinction coefficient spectra of all species involved in the photochemical changes and the relevant quantum yields which were assumed to be wavelength independent over the wavelength ranges of the different light sources. No systematic differences were found in the best-fit quantum yields derived from different experimental runs using either high concentrations and short path lengths or low concentrations and long path lengths and when using the different light sources.

Using the extinction coefficient spectra and quantum yields estimated in this way, we have been able to model the irradiation-induced evolution of the spectra of more complex types of sunscreen films. Firstly, in solution films containing a mixture of photo-unstable UV filter plus a photostable, "spectator" UV filter, light absorption by the spectator species slows down the photochemical reaction of the photo-unstable species. Secondly, we show how to model the spectra during irradiation of photo-unstable UV filters dissolved in emulsion films which scatter as well as absorb light. In addition to the issues resulting from light scattering, modelling the behaviour in emulsion films involves consideration of the partitioning of the dissolved UV filter between the immiscible liquid phases of the emulsion. Despite the rather high uncertainties in the final set of quantum yields and the assumption that they are wavelength independent, we observe very good agreement between calculated and measured spectra during irradiation for these more complex types of sunscreen film.

The data sets of the extinction coefficient spectra and the quantum yields enable use of the models developed above to explicitly predict the evolution of sunscreen spectra and derived SPF for different types of sunscreen films (solution or emulsions) during irradiation with "standard" sunlight. This ability to predict the behaviour under "standard" solar irradiation of sunscreen films containing any operator-set concentrations of one or more UV filters and values of other formulation variables such as emulsion composition significantly enhances the capability for the rational design and optimisation of sunscreen formulations. The key achievement of the work described here is that we have extended the existing ability to predict only the *initial* SPF solely for non-scattering films to include the ability to predict the complete time variation of SPF due to "standard" solar irradiation for both solution films and scattering emulsion films. For the future, it is desirable to improve the accuracy of the quantum yield values reported here and to determine whether the assumption of wavelength independence of the quantum yields introduces a significant systematic error. In addition, measurement of extinction coefficient spectra and relevant quantum yields for a wider range of UV filters and solvents will extend the possible options for the rational design and property prediction of new sunscreen formulations. Finally, we note that solar irradiation is only one of three main factors which cause sunscreen films to change during use. In order to fully describe the time evolution of sunscreen films the factor relating to solar irradiation must be considered in parallel with factors due to water immersion and due to film evaporation [7,8].

Acknowledgements

We thank GlaxoSmithKline Consumer Healthcare for funding this work and supplying the samples of UV filters used here.

References

[1] B.L. Diffey, J. Robson, A new substrate to measure sunscreen protection factors throughout the ultraviolet spectrum J. Soc. Cosmet. Chem. 40 (1989) 127-133.
[2] B.L. Diffey, P.R. Tanner, P.J. Matts, F.J. Nash, In vitro assessment of the broad-spectrum ultraviolet protection of sunscreen products. J. Amer. Acad. Dermatol. 43 (2000) 1024-1035.
[3] U. Osterwalder, B. Herzog, Sun protection factors: world-wide confusion, Brit. J. Dermatol. 161 (2009) 13-24.
[4] A.W. Schmalwieser, S. Wallisch, B. Diffey, A library of action spectra for erythema and pigmentation. Photochem. Photobiol. Sci. 11 (2012) 251- 268.
[5] D. Moyal, V. Alard, C. Bertin, F. Boyer, M.W. Brown, L. Kolbe, P. Matts, M. Pissavini, The revised COLIPA in vitro UVA method. Int. J. Cosmetic Sci. 35 (2013) 35-40.
[6] D.M. Beyer, A. Faurschou, P.A. Philipsen, M. Hoedersdal, H.C. Wulf, Sun protection factor persistence on human skin during a day without physical activity or ultraviolet exposure. Photodermatol., Photoimmunol & Photomed. 26 (2010) 22-27.
[7] B.P. Binks, J. Brown, P.D.I. Fletcher, A.J. Johnson, I. Marinopoulos, J.M. Crowther, M.A. Thompson, Evaporation of sunscreen films: how the UV protection properties change. ACS App. Mater. Interfaces 8 (2016) 13270-13281.
[8] Evaporation of particle-stabilised emulsion sunscreen films. B.P. Binks, P.D.I. Fletcher, A.J. Johnson, I. Marinopoulos, J. Crowther and M. Thompson, ACS App. Mater. & Interfaces 8 (2016) 21201-21213.
[9] U.S. Department of Health and Human Services, Food and Drug Administration, Center for Drug Evaluation and Research (CDER), Guidance for Industry. Labeling and Effectiveness Testing: Sunscreen Drug Products for Over-The-Counter Human Use — Small Entity Compliance Guide, December 2012.
[10] B. Herzog, M. Wehrle, K. Quass, Photostability of UV absorber systems in sunscreens. Photochem. Photobiol. 85 (2009) 869-878.
[11] J. Stanfield, U. Osterwalder, B. Herzog, In vitro measurements of sunscreen protection. Photochem. Photobiol. Sci. 9 (2010) 489-494.
[12] J. Hojerova, A. Medovcikova, M. Mikula, Photoprotective efficacy and photostability of fifteen sunscreen products having the same label SPF subjected to natural sunlight, Int. J. Pharm. 408 (2011) 27-38.
[13] J. Kockler, M. Oelgemoller, S. Robertson, B.D. Glass, Photostability of sunscreens, J. Photochem. Photobiol. C 13 (2012) 91-110.
[14] N.A. Shaath, Ultraviolet filters. Photochem. Photobiol. Sci. 9 (2010) 464-469.
[15] C. Stiefel, W. Schwack, Y.T. Nguyen, Photostability of cosmetic UV filters on mammalian skin under UV exposure. Photochem. Photobiol. 91 (2015) 84-91.
[16] C.F. Bohren, D.R. Huffman, Absorption and scattering of light by small particles. Wiley VCH, Weinheim (2004).
[17] W.A. Noyes, The Photochemistry of Gases, Reinhold Pub. Corp., New York, (1941).
[18] J.G. Calvert, J.N. Pitts Jr., Photochemistry, Wiley and Sons, New York, (1966).
[19] H.J. Kuhn, S.E. Braslavsky, R. Schmidt, Chemical actinometry (IUPAC Technical Report). Pure Appl. Chem. 76 (2004) 2105-2146.
[20] H.J. Adick, R. Schmidt, H.D. Brauer, Two wavelength-independent chemical actinometers which together cover the range 334-500 nm. J. Photochem. Photobiol. A 45 (1988) 89-96.
[21] W. Schwack, T. Rudolph, Photochemistry of dibenzoyl methane UVA filters. Part 1. J. Photochem. Photobiol. B 28 (1995) 229-234.
[22] M. Dubois, P. Gilard, P. Tiercet, A. Deflandre, M.A. Lefebvre, J. Chim. Phys. 95 (1998) 388-394.

[23] N. Tarras-Wahlberg, G. Stenhagen, O. Larko, A. Rosen, A-M. Wennberg, O. Wennerstrom, Changes in ultraviolet absorption of sunscreen after ultraviolet irradiation. J. Inv. Dermatol. 113 (1999) 547-553.
[24] E. Chatelain, B. Gabard, Photostabilization of butly methoxydibenzoylmethane (avobenzone) and ethylhexyl methoxycinnamate by bis-ethylhexyloxyphenol methoxyphenol triazine (Tinosorb S), a new UV broadband filter. Photochem Photobiol. 74 (2001) 401-406.
[25] A. Cantrell, D.J. McGarvey, Photochemical studies of 4-tert-butyl-4'-methoxydibenzoylmethane (BM-DBM). J. Photochem. Photobiol. B 64 (2001) 117-122.
[26] A. Aspee, C. Allaga, J.C. Scaiano, Transient enol isomers of dibenzoylmethane and avobenzone as efficient hydrogen donors towards a nitroxide pre-fluorescent probe. Photochem. Photobiol. 83 (2007) 481-485.
[27] G.J. Mturi, B.S. Matincigh, Photostability of the sunscreening agent 4-tert-butyl-4'methoxydibenzoylmethane (avobenzone) in solvents of different polarity and proticity, J. Photochem. Photobiol. A, 200 (2008) 410-420.
[28] C. Paris, V. Lhiaubet-Vallet, O. Jiminez, C. Trullas, M.A. Mirnada, A blocked diketo form of avobenzone: photostability, photosentizing properties and triplet quenching by a triazine-derived UVB filter. Photochem. Photobiol. 85 (2009) 178-184.
[29] B. Herzog, M. Wehrle, K. Quass, Photostability of UV absorber systems in sunscreens, Photochem. Photobiol. 85 (2009) 869-878.
[30] V. Lhiaubet-Vallet, M. Marin, O. Jiminez, O. Gorchs, C. Trullas, M.A. Miranda, Filter-filter interactions. Photostabilization, triplet quenching and reactivity with singlet oxygen. Photochem. Photobiol. Sci. 9 (2010) 552-558.
[31] J.J. Vallejo, M. Meas, C. Gallardo, Evaluation of the avobenzone photostability in solvents used in cosmetic formulations, Vitae, Rev. Fac. Quim. Farm. 18 (2011) 63-71.
[32] J. Zawadiak, M. Mrzyczek, Influence of substituent on UV absorption and keto-enol tautomerism equilibrium of dibenzoylmethane derivatives. Spectrochim. Acta A 96 (2012)815-819.
[33] M. Yamaji, M. Kida, Photothermal tautomerism of a UV sunscreen (4-tert-butyl-4'-methoxydibenzoylmethane) in acetonitrile studied by flash photolysis. J. Phys. Chem. A117 (2013) 1946-1951.
[34] P. Morliere, O. Avice, T.S.E. Melo, L. Dubertret, M. Giraud, R. Santus, A study of the photochemical properties of some cinnamate sunscreens by steady state and laser flash photolysis. Photochem. Photobiol. 36 (1982) 395-399.
[35] S. Pattanaargson, T. Munhapol, P. Hirunsupachot, P. Luangthongaram, Photoisomerization of octyl methoxycinnamate. J. Photochem. Photobiol. A 161 (2004) 269-274.
[36] S.P. Huong, V. Andrieu, J-P. Reynier, E. Rocher, J-D. Fourneron, The photosimerization of the sunscreen ethylhexyl p-methoxy cinnamate and its influence on the sun protection factor. J. Photochem. Photobiol. A 186 (2007) 65-70.
[37] T.M. Karpkird, S. Wanichweachharungruang, B. Albinsson, Photochem. Photobiol. Sci. 8 (2009) 1455-1460.
[38] L.A. MacManus-Spencer, M.L. Tse, J.L. Klein, A.E. Kracunas, Aqueous photolysis of the organic ultraviolet filter chemical octyl methoxycinnamate. Environ. Sci. Technol. 45 (2011) 3931-3937.
[39] K.M. Hanson, S. Narayanan, V.M. Nichols, C.J. Bardeen, Photochemical degradation of the UV filter octyl methoxycinnamate in solution and in aggregates. Photochem. Photobiol. Sci. 14 (2015) 1607-1616.

[40] MiePlot version 4.5.01 downloaded from http://www.philiplaven.com/mieplot.htm
[41] Herzog, B.; Sengün, F. Scattering particles increase absorbance of dyes – a model study with relevance for sunscreens. *Photochem. Photobiol. Sci.* 14 (2015) 2054-2063.

Table 1. Quantum yields for the photochemical processes of AVB and MC in SQ and PG at 32ºC.

System	Quantum yield ϕ	Quantum yield ϕ
	Enol to keto	Keto to prod
AVB in SQ	$2\pm1 \times 10^{-4}$	$\sim2 \times 10^{-4}$
AVB in PG	$4\pm2 \times 10^{-5}$	$\sim2 \times 10^{-4}$
	Trans to cis	Cis to trans
MC in SQ	0.028 ± 0.009	0.10 ± 0.03
MC in PG	0.16 ± 0.05	1.0 ± 0.3

Table 2. Solubilities of the UV filters in squalane (SQ) and propane-1,2-diol (PG) at 32ºC (data from refs. 7 and 8).

	Solubility data at 32ºC		
UV absorbers	**Solvent**	**Solubility/mM**	**Solubility/wt.%**
AVB	squalane	38	1.45
AVB	propane-1,2-diol	14	0.42
BEMT	squalane	16	1.24
BEMT	propane-1,2-diol	<0.5	<0.03
DHHB	squalane	20	0.98
DHHB	propane-1,2-diol	28	1.07
MC	squalane	1300	39.8
MC	propane-1,2-diol	435	10.4

Table 3. Fitted values of the species' partition coefficients at 32ºC. The values in brackets correspond to the ratio of the equilibrium solubilities.

UV filter/emulsion type	**Partition coefficients at 32ºC**		
AVB	P_{enol}	P_{keto}	P_{prod}
5 mM AVB/SQ-in-PG	3.0 (2.7)	0.65	Set to 0
5 mM AVB/PG-in-SQ	3.0 (2.7)	1.0	Set to 0
MC	P_{trans}	P_{cis}	
8.38 mM MC/PG-in-SQ	1.4 (3.0)	5.2	
8.38 mM MC/SQ-in-PG	1.5 (3.0)	4.6	

Figure 1. Molecular structures of the UV filters used here.

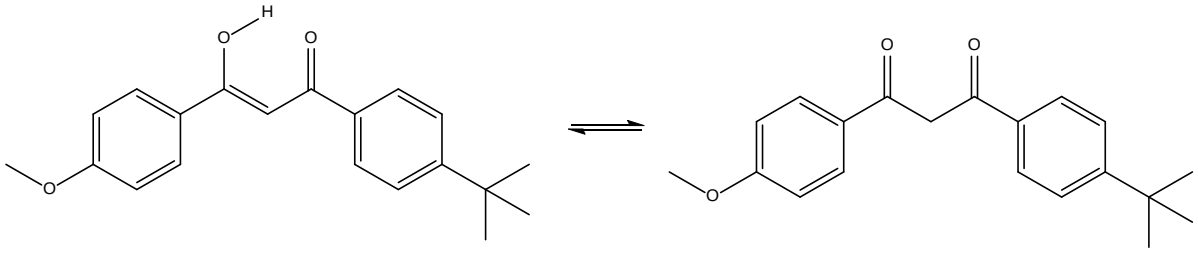

4-*tert*-butyl-4'-methoxy dibenzoyl methane (enol ⇌ keto forms) (AVB)

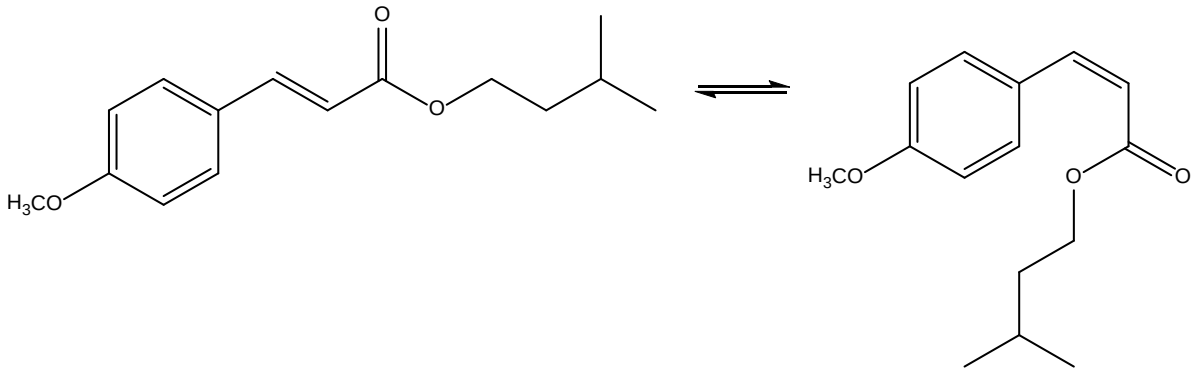

Iso-pentyl *p*-methoxycinnamate (trans ⇌ cis forms) (MC)

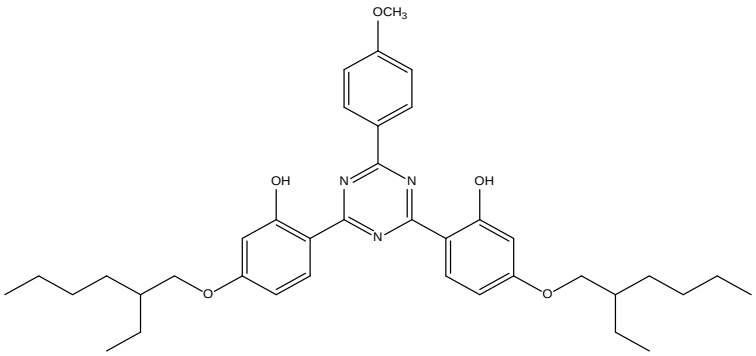

Bis-ethylhexyloxyphenol methoxyphenyl triazine (BEMT)

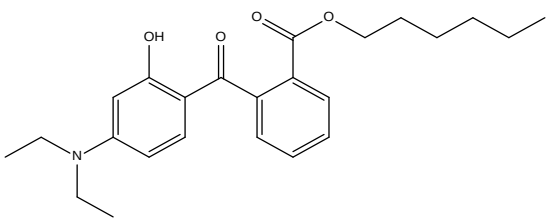

Diethylamino hydroxybenzoyl hexyl benzoate (DHHB)

Figure 2. Upper plot: spectra (versus air as reference) of 0.47 mM DMA in Freon 113 in a 1 cm path length cuvette during irradiation with the UV lamp at 14.4 cm. In order of decreasing peak size, the spectra correspond to 1 minute intervals for 0 – 20 min irradiation. Lower plot: derived spectral irradiances of the light sources used and standard sunlight.

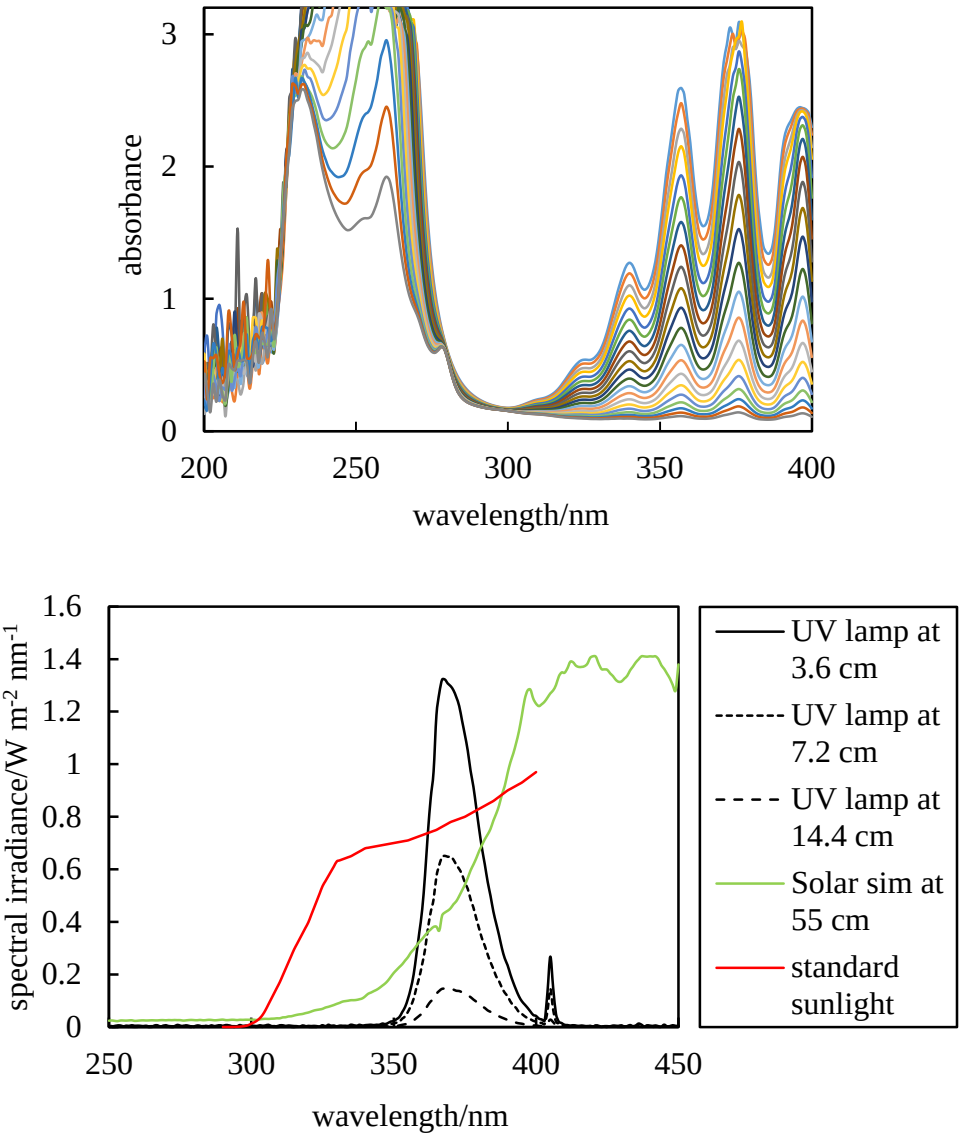

Figure 3. Upper plot: Spectra as a function of irradiation time (UV lamp at 7.2 cm) for 8 mM AVB in squalane with path length 0.01 cm. Middle plot: Species concentrations obtained by fitting the measured spectra shown above. Lower plot: Derived extinction coefficient spectra of the enol, keto and product species.

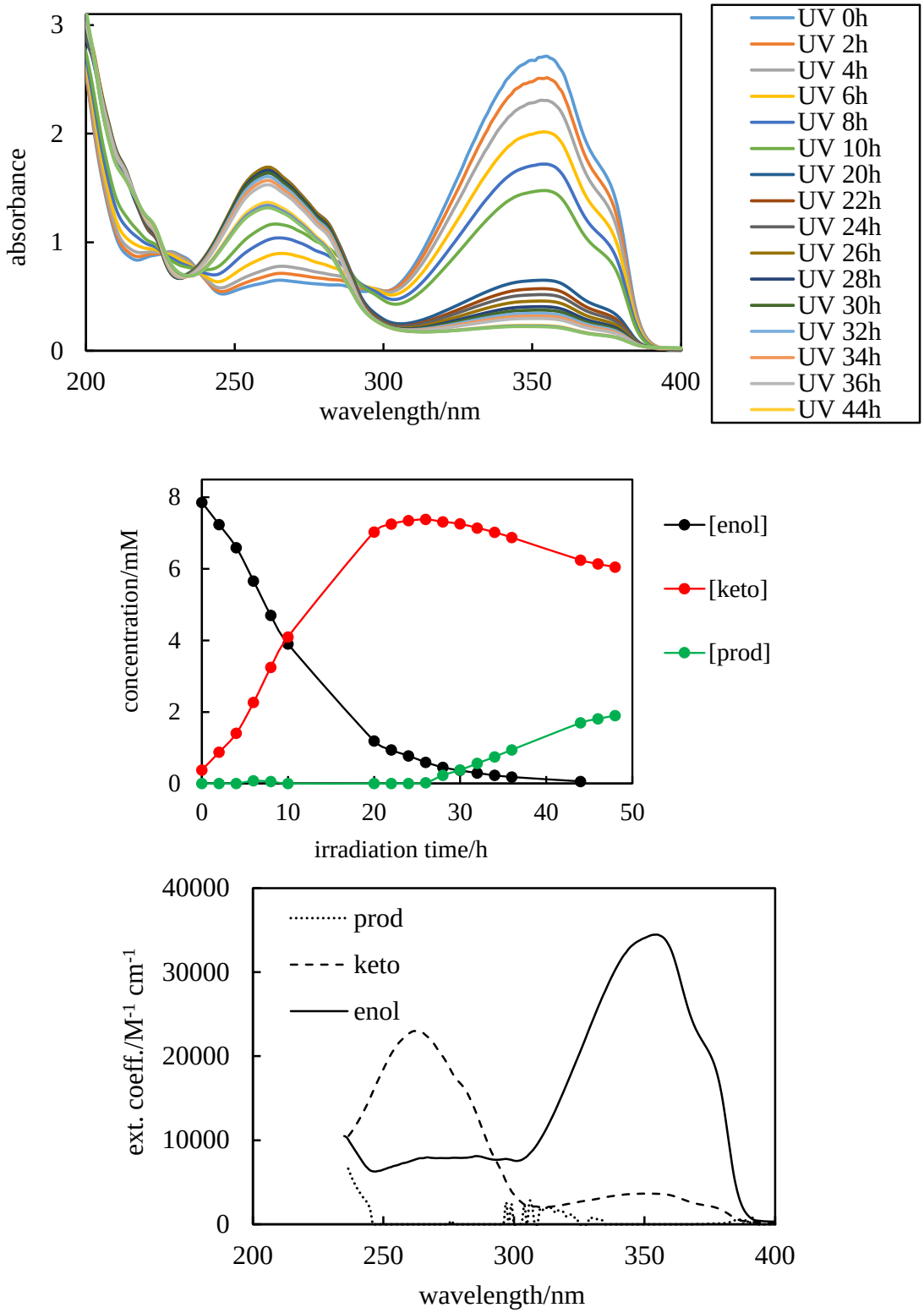

Figure 4. Comparison of measured (upper plot) and calculated (middle plot) spectra and SPF values (lower plot) for 12 mM AVB in squalane with 0.0018 cm path length as a function of irradiation time with the UV lamp at 7.2 cm.

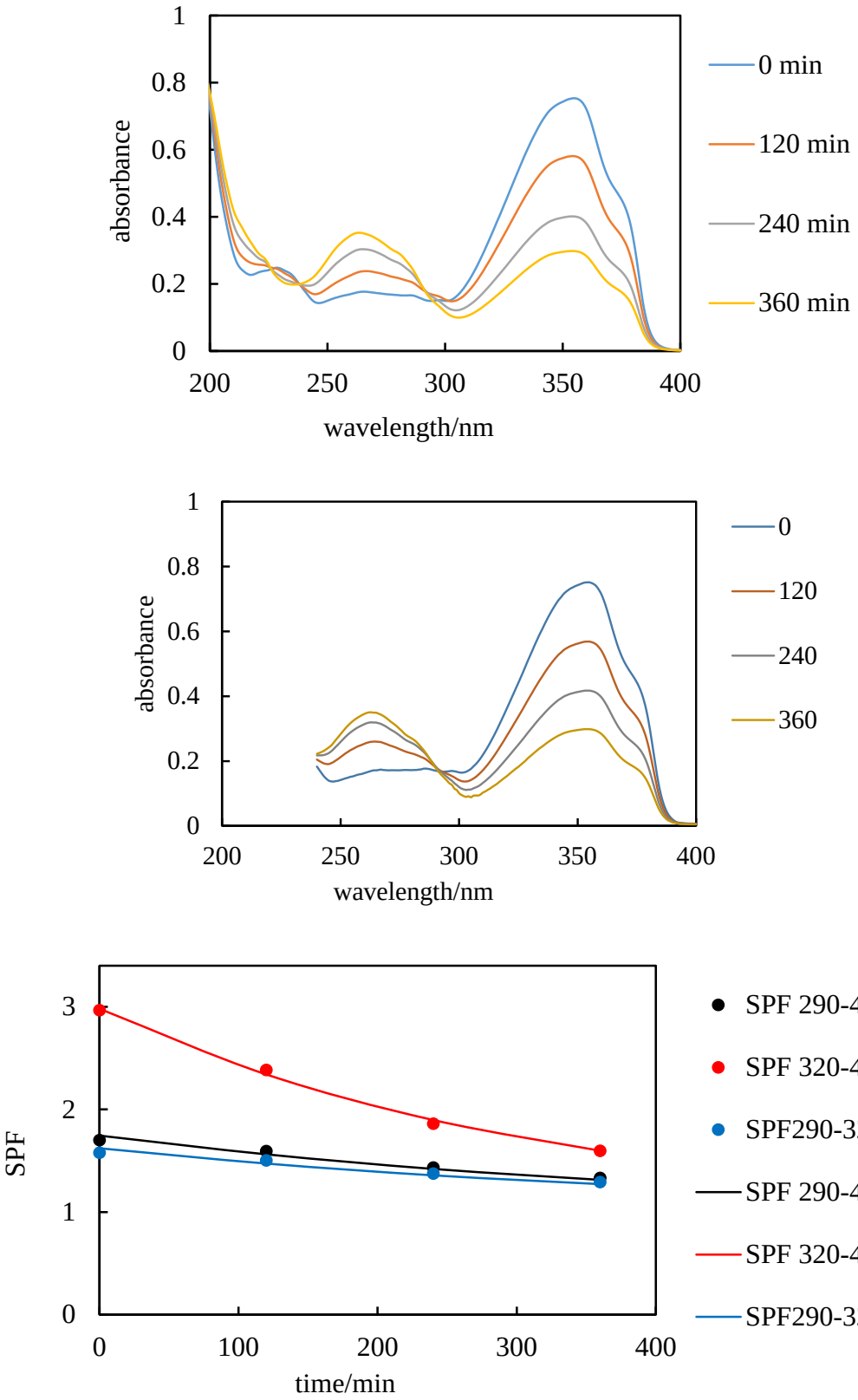

Figure 5. Upper plot: Spectra as a function of irradiation time (UV lamp at 14.4 cm) for 0.5 mM MC in PG with path length 0.1 cm. Middle plot: Species concentrations obtained by fitting the measured spectra shown above. Lower plot: Derived extinction coefficient spectra of the cis and trans species.

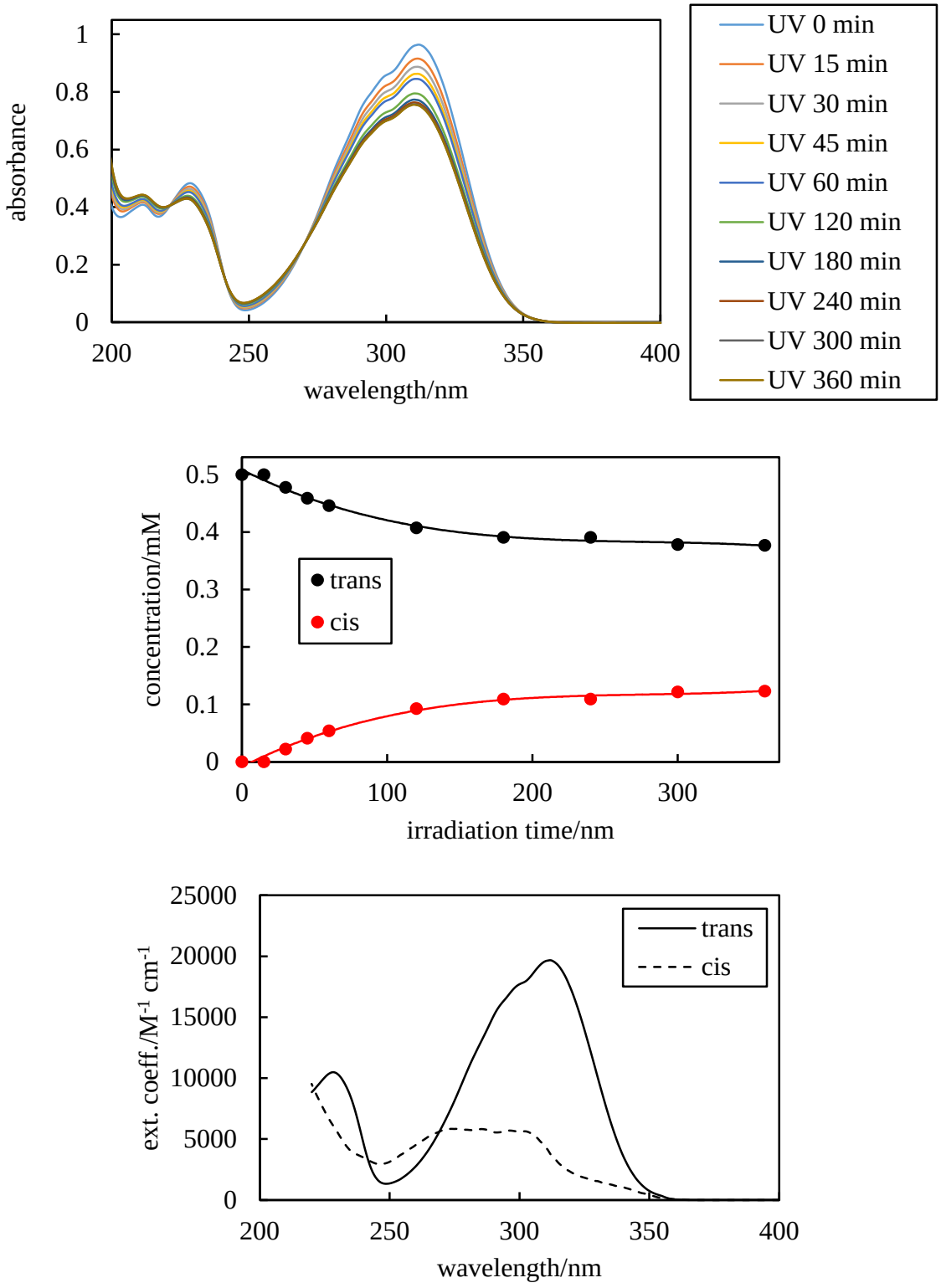

Figure 6. Comparison of measured (upper plot) and calculated (middle plot) spectra and SPF values (lower plot) for 6 mM MC in PG with 0.01 cm path length as a function of irradiation time with the UV lamp at 7.2 cm. The legend indicates the irradiation time in minutes.

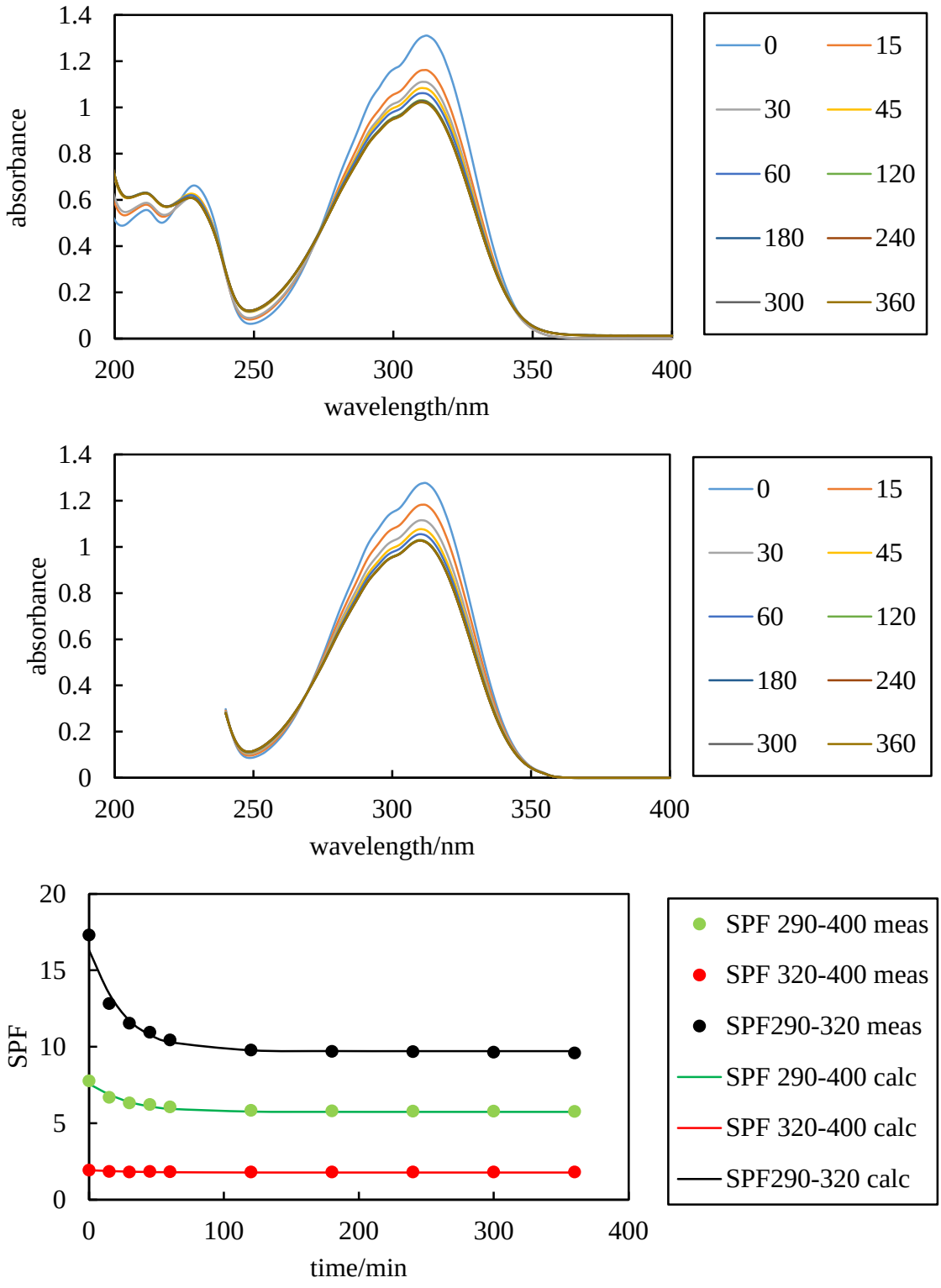

Figure 7. Comparison of measured (upper plot) and calculated (lower plot) spectra for 2.5 mM AVB plus 2.23 mM BEMT in SQ with 0.01 cm path length as a function of irradiation time with the UV lamp at 7.2 cm. The legend indicates the irradiation time in hours.

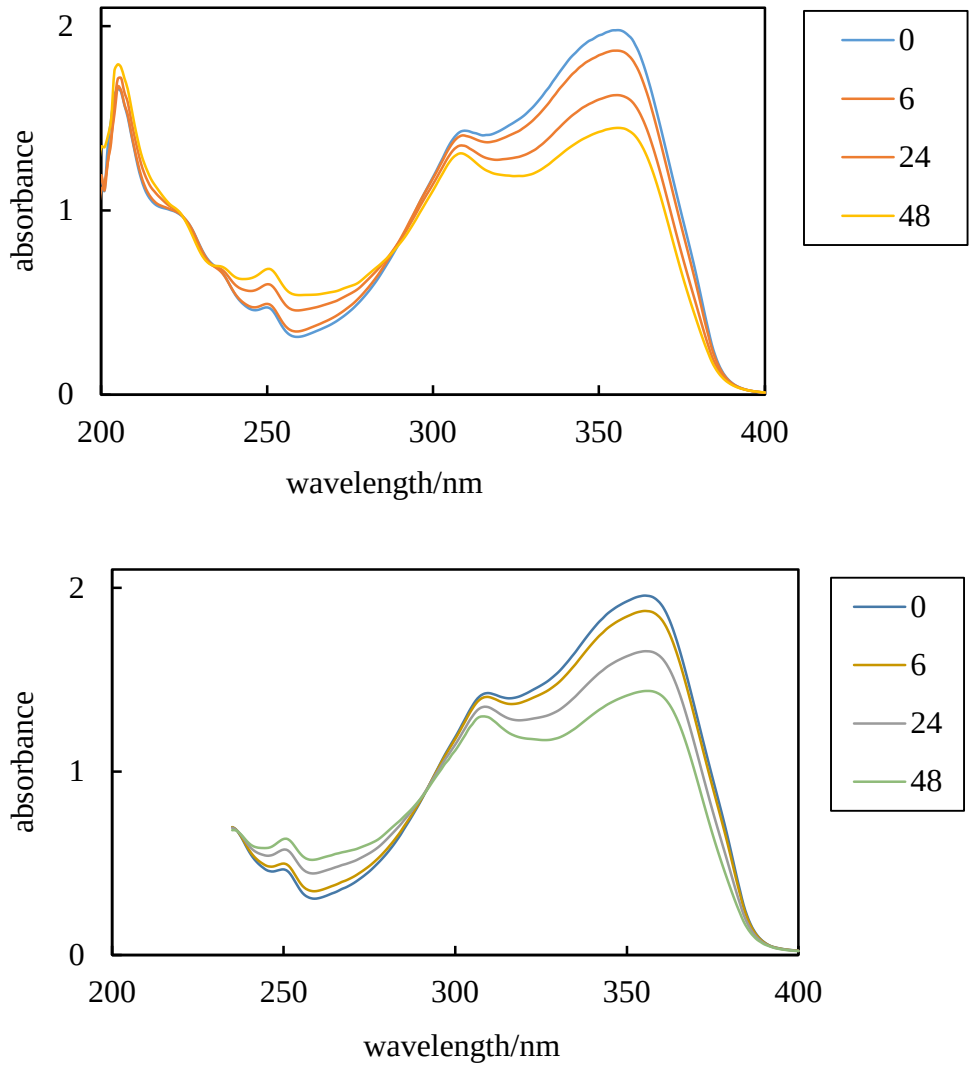

Figure 8. Upper plot: Comparison of calculated (lines) and measured (points) variation of SPF 2.5 mM AVB (solid lines and filled points) and 2.5 mM AVB plus 2.23 mM BEMT (dashed lines and empty points) in SQ with 0.01 cm path length as a function of irradiation time with the UV lamp at 7.2 cm. Lower plot: Variation of the concentrations of the enol, keto and product species for the same systems.

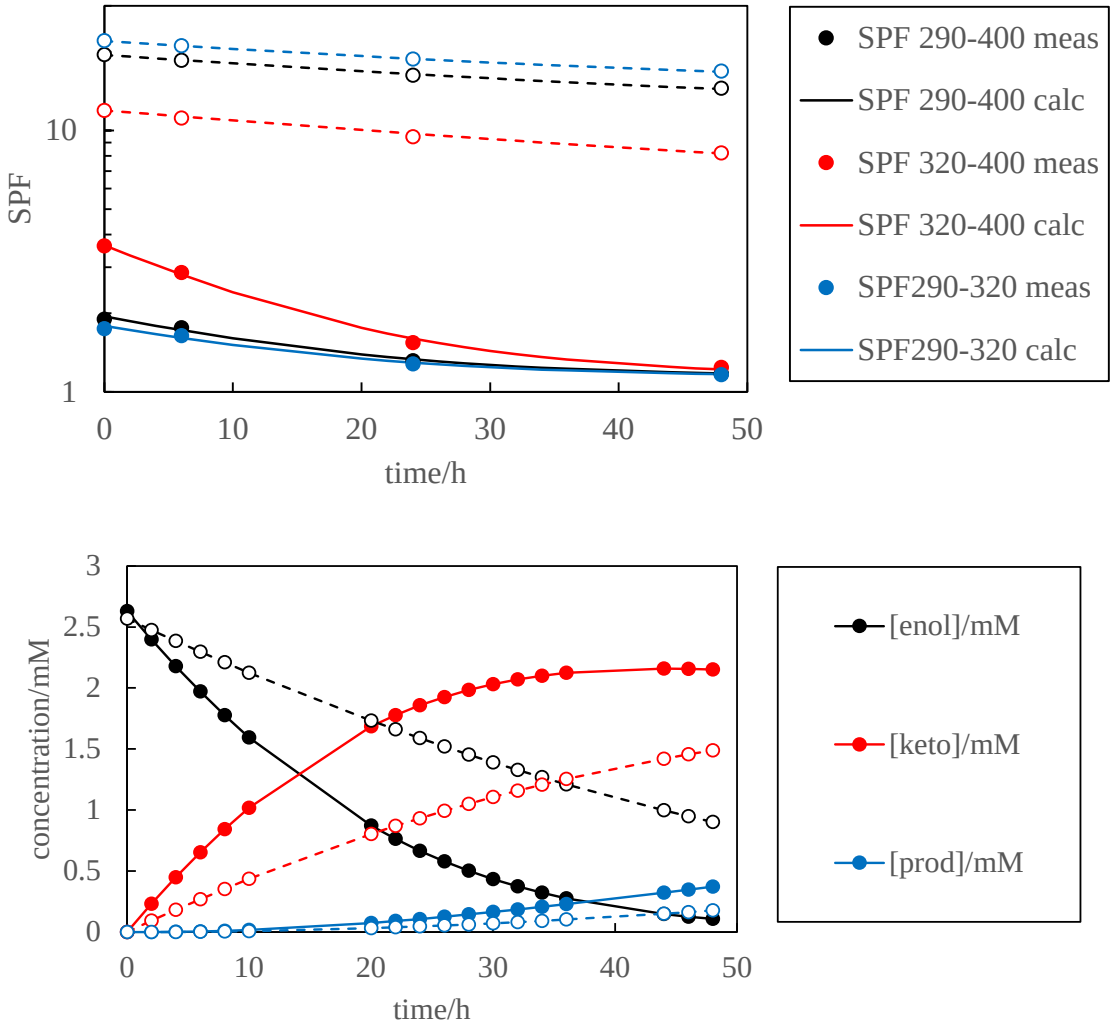

Figure 9. Upper image: SQ-in-PG emulsion with 50 vol% PG, no dissolved UV filter, mean droplet diameter equal to approx. 20 μm and stabilised by 1 wt% of 35 %SiOH silica particles. Lower image: PG-in-SQ emulsion with 50 vol% PG, no dissolved UV filter, mean droplet diameter equal to approx. 18 μm and stabilised by 1 wt% of 23 %SiOH silica particles.

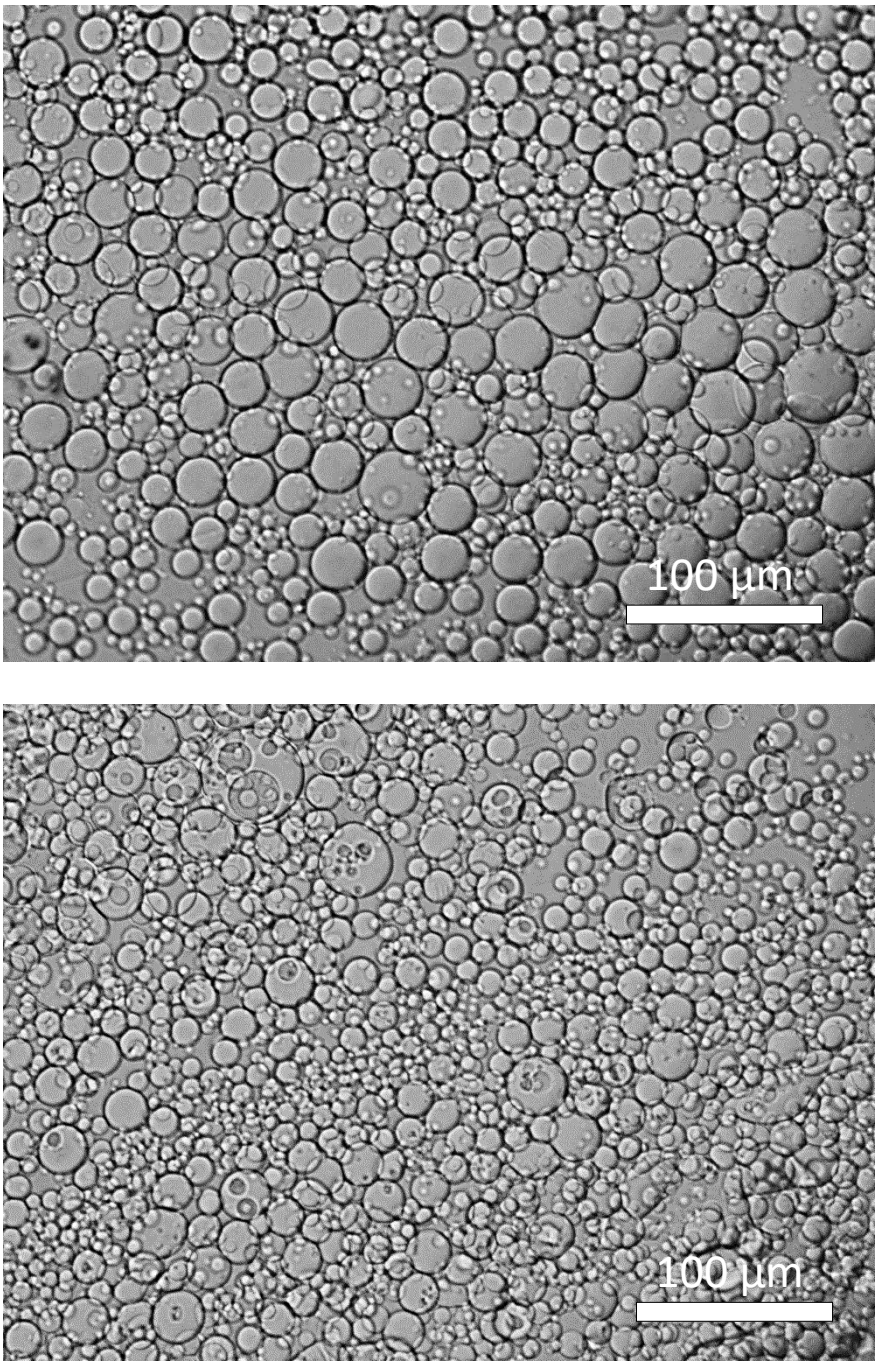

Figure 10. Comparison of measured (upper plot) and calculated (middle plot) spectra for 5 mM AVB in a SQ-in-PG emulsion with 50 vol% PG, stabilised with 1 wt% of 35 %SiOH silica particles and 0.01 cm path length as a function of irradiation time with the UV lamp at 7.2 cm. The legend indicates the irradiation time in hours. The dashed lines shows the measured specular absorbance spectrum of the emulsion alone. The lower plot compares SPF values derived from the measured and calculated spectra.

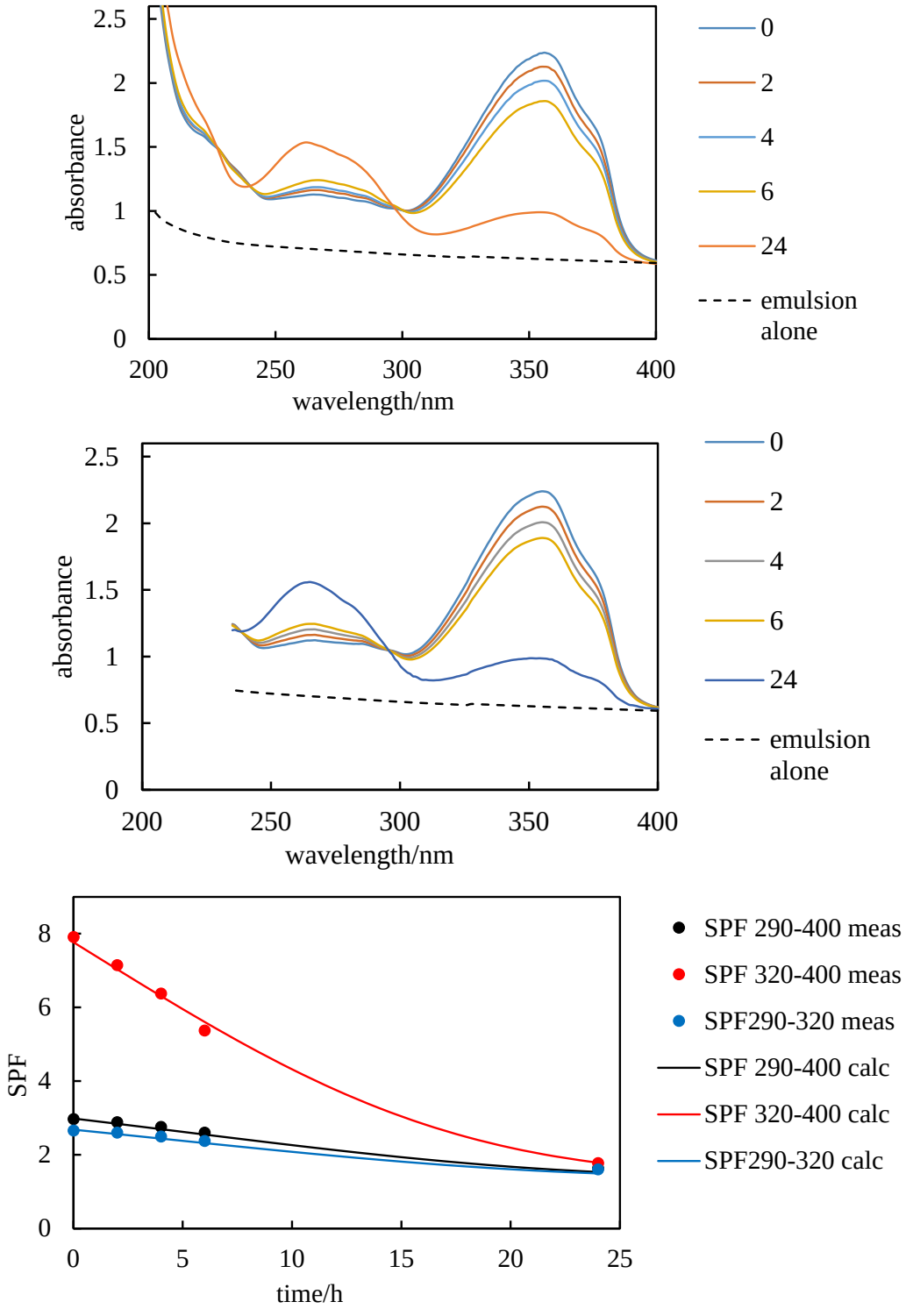

Figure 11. Variation of the averaged values of initial photochemical rates for AVB (upper plot) and the measured first-order rate constants for MC photo-isomerisation (lower plot) in emulsions with different volume fractions of PG. The plots refer to irradiation with the UV lamp at 7.2 cm. The solid lines are calculated as described in the text.

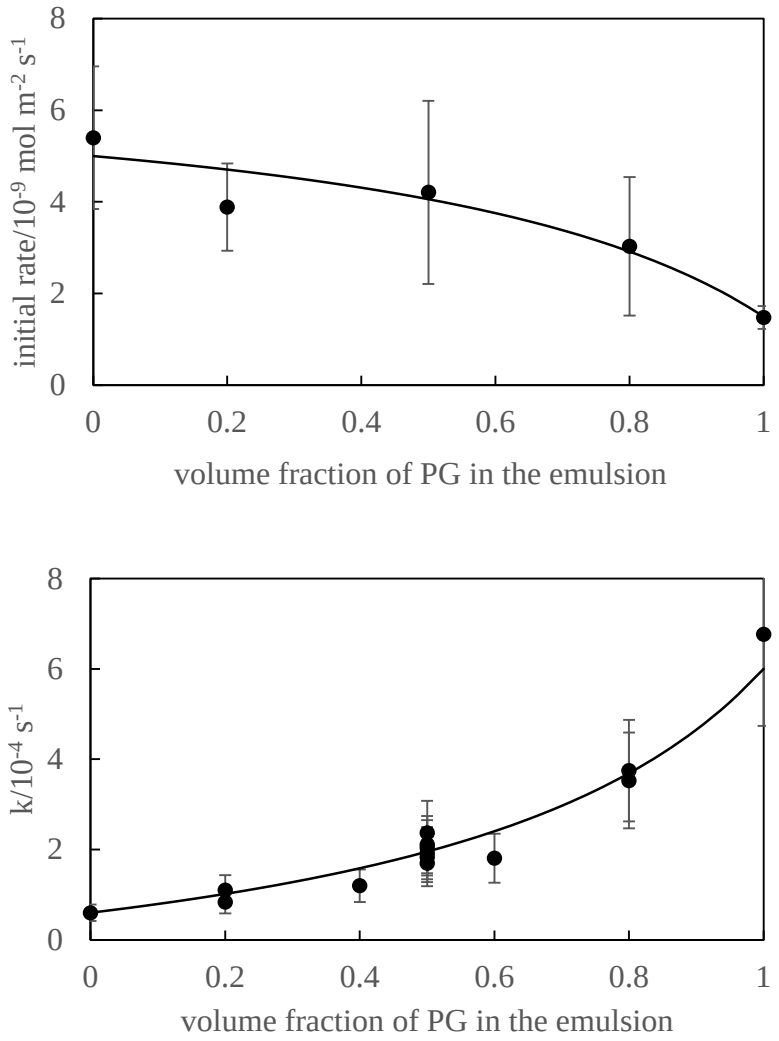

Figure 12. Calculated evolution of the film spectrum (upper plot, SQ as solvent only, 20 min intervals), SPF and species concentrations during "standard" solar irradiation. The films contain 30 mM AVB in either SQ (solid lines) or PG (dashed lines) with a path length of 20 μm.

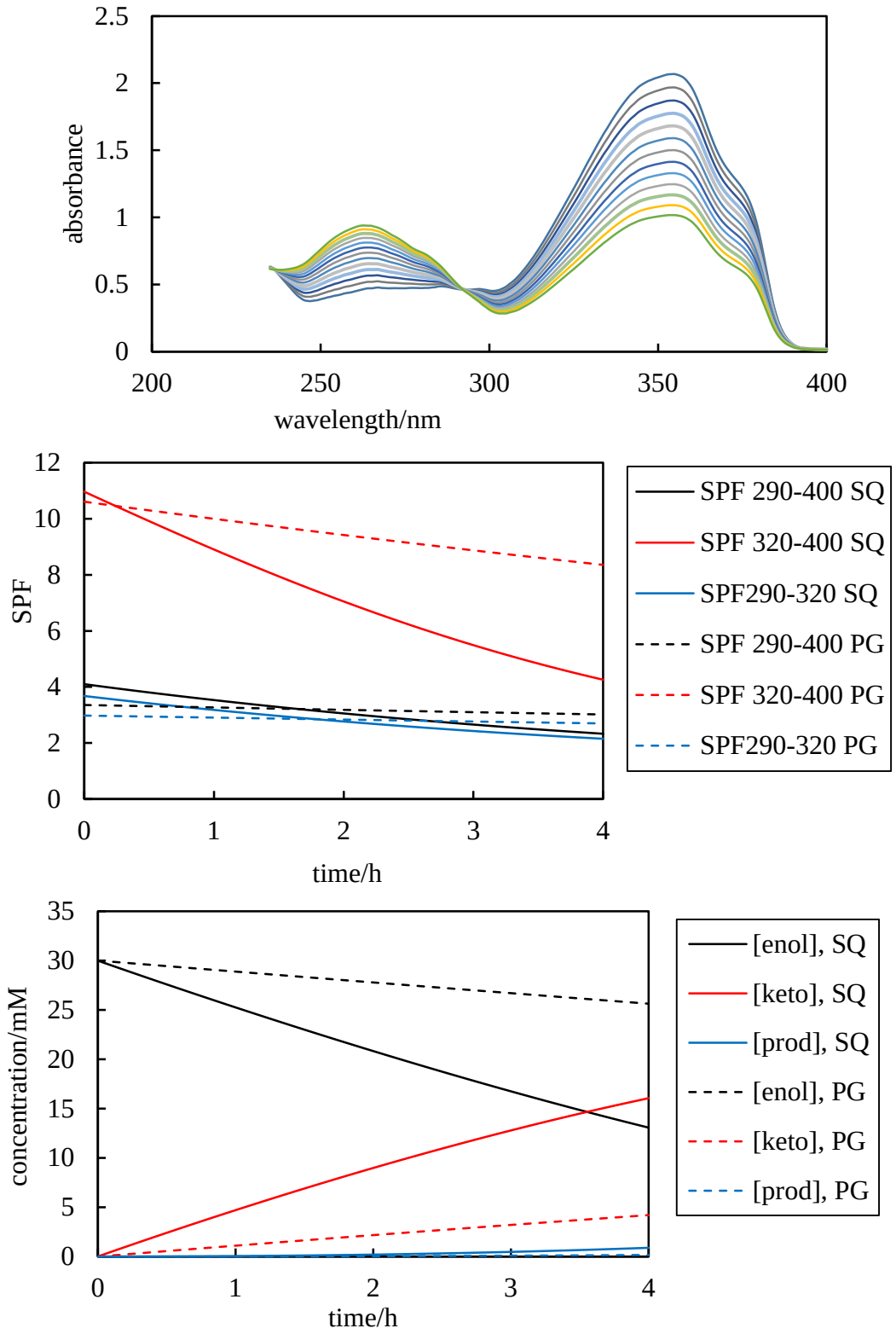

Figure 13. Calculated evolution of the film spectrum (upper plot, PG as solvent only, 50 s intervals), SPF and species concentrations during “standard” solar irradiation. The films contain 30 mM MC in either SQ (dashed lines) or PG (solid lines) with a path length of 20 μm.